

# Landslide tsunamis propagating around a conical island

E. RENZI AND P. SAMMARCO†

Dipartimento di Ingegneria Civile, Università degli Studi di Roma Tor Vergata, Via del Politecnico 1,  
00133 Roma, Italy

(Received 4 May 2009; revised 20 November 2009; accepted 22 November 2009;  
first published online 18 March 2010)

An analytical forced two-horizontal-dimension model is derived to investigate landslide tsunamis propagating around a conical island lying on a flat continental platform. Separation of variables and Laplace transform are used to obtain the free-surface elevation in the whole domain and the runup at the shoreline in terms of confluent Heun functions. The main properties of these functions and their asymptotic behaviour for large parameters are investigated. Expression of the transient leading wave travelling offshore is also derived. The distinguishing physical features of landslide tsunamis propagating in a round geometry are then pointed out and compared with those of landslide tsunamis propagating along a straight coast. Analytical results satisfactorily agree with available experimental data.

---

## 1. Introduction

The occurrence of some destructive events, such as the landslide tsunami of the Stromboli island (2002, Italy, South Mediterranean Sea) has recently renewed the interest in studying tsunamis propagating around islands (see Tinti *et al.* 2005). In the literature, the first known event of coastal inundation by tsunamis is dated back to 1620 BC, referring to the eruption of the Thera volcano in the eastern Mediterranean (see Bruins *et al.* 2008). Several similar tsunamis occurred through the centuries, like the devastating Krakatau island tsunami of 1883 (see Bruins *et al.* 2008) or the more recent Hokkaido island tsunami of 1993 (see Liu *et al.* 1995). Among these, the 1992 Flores island tsunami is of great interest, mostly because of the unexpectedly large runup reached in the lee side of the Babi island (Yeh *et al.* 1994; Bardet *et al.* 2003). Such recurring events led several authors to investigate on the scattering of incident long waves by circular islands (see Lautenbacher 1970; Smith & Sprinks 1975; Zhang & Zhu 1994; Fujima *et al.* 1995; Kanoglu & Synolakis 1998; Mei, Stiassnie & Yue 2005; Synolakis *et al.* 2008). Lautenbacher (1970) analysed the refractive influence of the bottom topography on tsunami runup around a conical island. He did not solve analytically the long-wave equation of motion, but transformed it into an integral form, which he eventually solved numerically. With this methodology, Lautenbacher (1970) showed that island runup can exceed runup of monodimensional plane beaches if the tsunami wavelength  $\lambda$  is comparable to the island diameter  $L$ , i.e.  $\lambda/L \simeq 1$ . Later on, Zhang & Zhu (1994) studied the propagation of water waves over variable depths in

† Email address for correspondence: sammarco@ing.uniroma2.it

a circular geometry and found a so-called ‘new’ solution to the problem. They presented a transformation of the original equation and then provided a power series solution. Nevertheless, the governing equation of motion studied by Zhang & Zhu (1994) is known as a confluent form of the Heun’s equation and had already been investigated long time ago (see Heun 1899). Then Fujima *et al.* (1995) described the characteristics of long-wave trapping around a conical island. They also solved the governing equation via the Frobenius power series expansion, but using a different and more complex transformation than that employed by Zhang & Zhu (1994). Finally Kanoglu & Synolakis (1998) developed an original analytical solution for long-wave runup around a conical island. Knowing the existing solution of the linear shallow-water wave equation for a cylinder over a flat bottom, Kanoglu & Synolakis (1998) were able to construct a conical island from sills. Then solved the long-wave equation for each of the sills separately, in terms of Bessel functions. Finally, they obtained the complete solution by matching the free-surface elevation and the fluxes at the geometrical discontinuities of the piecewise island. The methodology produced good comparison with laboratory data of Liu *et al.* (1995) in terms of time histories of free-surface elevation and maximum runup distribution around the island. Again, neither Fujima *et al.* (1995) nor Kanoglu & Synolakis (1998) recognized the governing equation to be a confluent form of the Heun equation (Heun 1899). However, note that Zhang & Zhu (1994), Fujima *et al.* (1995) and Kanoglu & Synolakis (1998) started their investigations before Slavjanov (1995) had formally developed and tuned the theory of confluent Heun equations (CHEs). Several analytical studies of landslide generated tsunamis along a plane beach are also available in the literature, from the seminal work of Tuck & Hwang (1972), who first analysed and solved the one-dimensional forced long-wave equation, to the new one-dimensional model introduced by Liu, Lynett & Synolakis (2003) and the two-horizontal-dimension model of Sammarco & Renzi (2008).

On the other hand, the analysis of tsunamis directly generated on the coast of a round island and propagating around and from it has not been fully developed. Tinti & Vannini (1995) worked out an analytical model of long waves propagating around a circular island lying over a flat bottom and enclosed in a large but finite ocean basin. The perturbation was induced by a bottom displacement occurring in the proximities of the island itself. A null free-surface elevation condition was imposed at the basin boundary, i.e. they assumed that the perturbation should decay at a finite distance from the island. As a consequence of this somewhat arbitrary assumption, Tinti & Vannini (1995) observed the occurrence of a local system of rotating edge waves, persisting long time after their generation. Indeed their results differ from those found earlier by Longuet-Higgins (1967), Meyer (1971) and Summerfield (1971): long waves propagating about a round island cannot be perfectly trapped. To show this fundamental result, simply consider the long-wave equation

$$g\nabla \cdot (h\nabla\zeta) = \frac{\partial^2\zeta}{\partial t^2}, \quad (1.1)$$

where  $g$  is the acceleration due to gravity,  $\nabla$  the nabla operator in polar coordinates  $(r, \theta)$ ,  $t$  time,  $\zeta$  the free-surface elevation and  $h = h(r)$  the water depth, to be specified further on. Now assume the free-surface elevation to be of the form  $\zeta(r, \theta, t) = \eta(r)e^{i(n\theta - \omega t)}$ , being  $i$  the imaginary unit and  $n \in \mathbb{N}$ ;  $\omega > 0$  is a given wave frequency. Under these assumptions the long-wave equation (1.1) can be written

in the Sturm-Liouville form

$$\frac{\partial}{\partial r} \left( hr \frac{\partial \eta}{\partial r} \right) + q(r)r\eta = 0, \quad (1.2)$$

with

$$q(r) = \frac{\omega^2}{g} - \frac{n^2 h}{r^2}. \quad (1.3)$$

The behaviour of the radial part  $\eta$  of the free-surface elevation is determined by the sign of the polynomial  $q(r)$ , expression (1.3). Hence  $\eta(r)$  will be oscillatory ( $q > 0$ ) or exponentially decreasing ( $q < 0$ ) following (see Mei *et al.* 2005):

$$\frac{\omega^2}{gn^2} \begin{cases} \geq \frac{h}{r^2}, & \text{oscillatory} \\ < \frac{h}{r^2}, & \text{exponential} \end{cases} \quad (1.4)$$

Now, assuming the water depth at infinity to be finite yields  $q(r) \simeq \omega^2/g > 0$  for large  $r$ . All the radial solutions  $\eta(r)$  to the governing equation (1.2) are oscillatory at large distances from the origin, even for small  $\omega$  (see Longuet-Higgins 1967; Meyer 1971; Mei *et al.* 2005). Hence perfect trapping is not possible in a polar-symmetric topography where  $h/r^2 \rightarrow 0$  as  $r \rightarrow \infty$ . As an application of the general theory exposed above, Summerfield (1971) studied the free-surface oscillations around a circular vertical island of radius  $r = a_1$  with a vertical edge at  $r = a_2 > a_1$ , lying on a continental shelf. Assuming again the free-surface elevation to be of the form  $\zeta(r, \theta, t) = \eta(r)e^{i(n\theta - \omega t)}$ , he solved the long-wave equation (1.1) separately for the two domains  $r < a_2$  and  $r > a_2$  respectively, in terms of Hankel functions. Then, by matching the two solutions at the common boundary  $r = a_2$ , he found the existence of a discrete set of complex eigenfrequencies  $\omega_{nm} = \xi_{nm} - i\epsilon_{nm}$ ,  $m \in \mathbb{N}$ , for each of the  $n$ th angular modes. These eigenfrequencies are characterized by a negative imaginary part, whose absolute value  $\epsilon_{nm}$  physically represents the rate of energy loss in time (damping factor). Modes with very small damping factor  $\epsilon_{nm}$  (for which energy leakage in time is small) were classified qualitatively as ‘almost trapped’ on the shelf; their amplitude was shown to attenuate exponentially while moving towards the ocean. On the other hand, modes with large  $\epsilon_{nm}$  were defined ‘leaky’, with a profile of a propagating wave to infinity. Regardless of the amount of damping, all the free modes propagate some amount of energy towards infinity. Hence, we infer that the free modes cannot be directly excited by local transient sources such as a landslide, which generates local perturbations not in the form of radiating waves to infinity. Indeed, the free modes of an island-shelf system could resonate only if excited by incoming wave trains (or travelling plane impulses, see Summerfield 1971). This observation has a counterpart with that of Meyer (1971), who noted that edge-wave modes on a sloping beach, due to their exponential decay in the offshore direction, can be excited only by local disturbances and not by waves incident from infinity (unless a nonlinear mechanism of subharmonic resonance is invoked, Guza & Davis 1974). In conclusion, for landslide-generated tsunamis propagating around a conical island, the free-surface elevation cannot be expressed neither as a system of rotating edge waves, nor in terms of the free modes of oscillation of the island-shelf system.

In §2, an analytical two-horizontal-dimension model of landslide tsunamis propagating around a conical island-shelf system is presented, based on the forced linear long-wave equation. The fluid domain is divided into a near field and a far field according to the discontinuities of the bottom slope. Separation of variables and the Laplace transform methods are employed to obtain the solutions of the

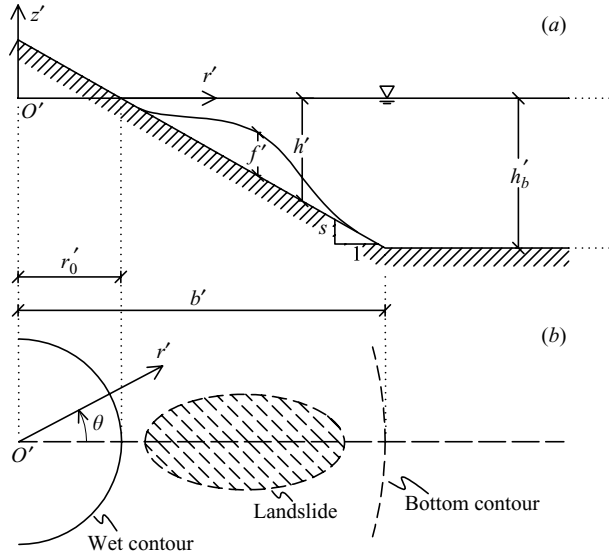


FIGURE 1. The fluid domain in physical coordinates. Radial section (a) and plan view (b) of the conical island, the continental platform and the landslide.

governing equations in terms of the free-surface elevation in each field. The two solutions are then matched at the common boundary. An analytical representation of the free-surface elevation is derived in each field, consisting in an integral form of an analytic function (confluent Heun for the near field and Hankel for the far field), multiplied by amplitude factors depending on the characteristics of the slide. In § 3, results obtained are shown to agree with the theoretical observations made by Meyer (1971) and summarized in Mei *et al.* (2005). The existence of a transient leading wave propagating outwards in the far field and decaying as  $O(t^{-1/2})$  is also shown. In § 4 the time series of the free-surface runup generated by a subaerial slide are satisfactorily compared with the available experimental results of Di Risio *et al.* (2009b). At the sampled points on the shoreline, the first incoming wave generated by the subaerial landslide is an elevation wave, followed by a deep trough, while the highest runup is reached by the second or third wave. This is due to the excitation of imperfect edge-wave-like components of the wave motion generated by the landslide. Finally, further investigation demonstrates that tsunamis propagating along a conical island generate smaller runup than those propagating along a plane beach with similar landslide characteristics. This is due to the energy leakage phenomenon always occurring with waves propagating in a round geometry.

## 2. Wave field

Consider a conical island of bottom radius  $b'$  lying on an indefinite horizontal continental platform; the island flanks have a uniform slope  $s$  (see figure 1). Let the primes denote physical dimensional quantities. In the cylindrical reference system  $(r', \theta, z')$  the  $r'$ -axis is directed radially, the  $z'$ -axis rises up from the undisturbed water level and  $\theta \in (-\pi, \pi)$  is the angular coordinate positive counter-clockwise. The origin  $O'$  is at the intersection of the undisturbed water level and the island vertical axis. Water is in the region  $r' > r'_0$ , being  $r'_0$  the radius of the wet contour located in the

upper part of the island. Assume that the landslide originates in a neighbourhood of the origin  $O'$  and is symmetric with respect to  $\theta$ .

2.1. The governing equations

In the whole fluid domain, consider the forced linear long-wave equation of motion in polar coordinates  $(r', \theta)$

$$\zeta'_{t't'} - gh' \left( \frac{1}{r'} \zeta'_{r'} + \zeta'_{r'r'} + \frac{1}{r'^2} \zeta'_{\theta\theta} \right) - gh'_{r'} \zeta'_{\theta} = f'_{t't'}, \tag{2.1}$$

where  $\zeta'(r', \theta, t')$  is the free-surface elevation and  $t'$  is the time. Subscripts denote differentiation with respect to the relevant variable. In (2.1),  $h'(r')$  is the overall bottom depth, in the absence of the landslide, measured with respect to the undisturbed water surface  $z' = 0$ . Hence  $h' = s(r' - r'_0)$  if  $r'_0 < r' < b'$ ;  $h' = s(b' - r'_0) \equiv h'_b$  if  $r' > b'$ , with  $h'_b$  the water head over the continental shelf. Finally,  $f'(r', \theta, t')$  is a time-dependent perturbation of the sea floor, representing the landslide moving along the flanks of the island (see figure 1). Now let  $\sigma$  and  $H$  be respectively the characteristic length and maximum vertical thickness of the landslide; then the following non-dimensional variables can be defined:

$$\left\{ \begin{matrix} r \\ r_0 \\ b \end{matrix} \right\} = \left\{ \begin{matrix} r' \\ r'_0 \\ b' \end{matrix} \right\} / \sigma, \quad t = \sqrt{\frac{gs}{\sigma}} t', \quad \left\{ \begin{matrix} \zeta \\ f \end{matrix} \right\} = \left\{ \begin{matrix} \zeta' \\ f' \end{matrix} \right\} / H, \quad h = \frac{h'}{\sigma s}. \tag{2.2}$$

The long-wave equation (2.1) becomes

$$\zeta_{tt} - h \left( \frac{1}{r} \zeta_r + \zeta_{rr} + \frac{1}{r^2} \zeta_{\theta\theta} \right) - h_r \zeta_r = f_{tt}. \tag{2.3}$$

Boundedness of the free-surface is required at every time in all the fluid domain:  $|\zeta(r, \theta, t)| < \infty$ . Zero initial free-surface elevation  $\zeta$  and velocity  $\zeta_t$  are also prescribed:  $\zeta(r, \theta, 0) = 0, \quad \zeta_t(r, \theta, 0) = 0$ . To solve the equation of motion (2.3) we employ the Laplace transform pair

$$\hat{\zeta}(r, \theta; \omega) = \int_0^\infty \zeta(r, \theta, t) e^{-\omega t} dt, \quad \zeta(r, \theta, t) = \frac{1}{2\pi i} \int_{c-i\infty}^{c+i\infty} \hat{\zeta}(r, \theta; \omega) e^{\omega t} d\omega, \tag{2.4}$$

where  $\omega = c + id$  is the complex non-dimensional transform parameter;  $c > 0$  is a real constant, large enough so that the integrals in (2.4) exist. Transform of (2.3) gives

$$r^2 \hat{\zeta}_{rr} + r \left( 1 + r \frac{h_r}{h} \right) \hat{\zeta}_r - \frac{\omega^2 r^2}{h} \hat{\zeta} + \hat{\zeta}_{\theta\theta} = -\frac{r^2}{h} \hat{f}_{tt}, \tag{2.5}$$

where

$$\hat{f}_{tt} = \int_0^\infty f_{tt}(r, \theta, t) e^{-\omega t} dt$$

is the Laplace transform of the forcing term  $f_{tt}$  of the governing equation (2.3). Referring to the whole fluid domain as sketched in figure 1, we shall define the *near field* as the domain where  $r_0 < r < b$ , and the *far field* the remaining indefinite region  $r > b$ . The equation of motion (2.5) will be solved in each field separately, starting from the near field and then moving to the far field. The two solutions will be matched afterwards at the boundary  $r = b$ .

## 2.2. Solution of transformed equation

2.2.1. The near field  $r_0 < r < b$ 

In the near field  $h = r - r_0$ , then (2.5) becomes

$$r^2 \hat{\xi}_{rr} + r \left( 1 + \frac{r}{r - r_0} \right) \hat{\xi}_r - \frac{\omega^2 r^2}{r - r_0} \hat{\xi} + \hat{\xi}_{\theta\theta} = -\frac{r^2}{r - r_0} \hat{f}_{tt}, \quad (2.6)$$

which is an inhomogeneous second order partial differential equation. To obtain its solution, let us consider the associated homogeneous equation

$$r^2 \hat{\xi}_{rr} + r \left( 1 + \frac{r}{r - r_0} \right) \hat{\xi}_r - \frac{\omega^2 r^2}{r - r_0} \hat{\xi} + \hat{\xi}_{\theta\theta} = 0. \quad (2.7)$$

Separation of variables  $\hat{\xi}(r, \theta; \omega) = R(r; \omega)\Theta(\theta)$  yields  $\Theta_n(\theta) = \cos n\theta$ ,  $n = 0, 1, 2, \dots$  for the angular part  $\Theta$ , having required  $\Theta$  to be a periodic function of period  $2\pi$  and to be symmetric with respect to  $\theta = 0$ . Back to the homogeneous equation, separation of variables yields the following ordinary differential equation for the radial function  $R = R_n(r; \omega)$ :

$$R_{n,rr} + \left( \frac{1}{r} + \frac{1}{r - r_0} \right) R_{n,r} + \left[ \frac{(i\omega)^2}{r - r_0} - \frac{n^2}{r^2} \right] R_n = 0, \quad (2.8)$$

which is a CHE in its natural general form (see Slavyanov 1995),  $r$  being the independent variable and  $(i\omega)$  a complex parameter. Solution of (2.8) can be found by applying the Frobenius method of power series, as shown in §A.1, thus obtaining

$$R_n(r; i\omega) = \alpha_n Hc_n^{(1)}(r; i\omega) + \beta_n Hc_n^{(2)}(r; i\omega),$$

$\alpha_n$  and  $\beta_n$  being the integration constants.  $Hc_n^{(1,2)}$  are the confluent Heun functions of order  $n$  of (first and second) kind (see §A.1) respectively:

$$Hc_n^{(1)}(r; i\omega) = \sum_{m=0}^{\infty} a_{nm}(i\omega) \left( 1 - \frac{r_0}{r} \right)^m, \quad (2.9)$$

and

$$Hc_n^{(2)}(r; i\omega) = \ln \left( 1 - \frac{r_0}{r} \right) Hc_n^{(1)}(r; i\omega) + \sum_{m=0}^{\infty} b_{nm}(i\omega) \left( 1 - \frac{r_0}{r} \right)^m, \quad (2.10)$$

where parametric dependence on the radius  $r_0$  is omitted for brevity. The series coefficients  $a_{nm}$  in (2.9) and  $b_{nm}$  in (2.10) are given respectively by

$$a_{nm}(i\omega) = \frac{1}{m^2} \sum_{k=1}^m a_{n,m-k} \left[ n^2(k-1) + \frac{\omega^2 r_0}{2} (k+k^2) \right]$$

and

$$b_{nm}(i\omega) = \frac{1}{m^2} \sum_{k=1}^m b_{n,m-k} \left[ n^2(k-1) + \frac{\omega^2 r_0}{2} (k+k^2) \right] - \frac{2}{m} a_{nm},$$

with  $m = 1, 2, \dots$ ,  $a_{n0} = 1$  and  $b_{n0} = 0$ . Since the confluent Heun function of the second kind  $Hc_n^{(2)}$  has a logarithmic singularity for  $r \rightarrow r_0$  (see 2.10), boundedness of the free-surface elevation at  $r = r_0$  is satisfied only if  $\beta_n = 0$ . Hence

$$R_n(r; \omega) = \alpha_n Hc_n^{(1)}(r; i\omega). \quad (2.11)$$

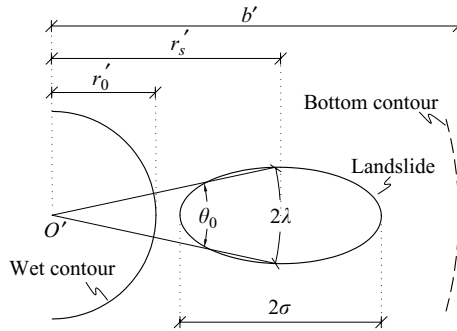


FIGURE 2. Landslide specifications.  $\sigma$  and  $\lambda$  are the characteristic dimensions of the slide, while  $\theta_0 = 1/\gamma$  is the characteristic angle subtended by the slide with respect to the origin of the reference system.

The solution  $\hat{\zeta}_h$  of the homogeneous equation (2.7) associated to (2.6) is then

$$\hat{\zeta}_h(r, \theta, t) = \sum_{n=0}^{\infty} \alpha_n R_n(r; \omega) \Theta_n(\theta) = \sum_{n=0}^{\infty} \alpha_n Hc_n^{(1)}(r; i\omega) \cos n\theta. \tag{2.12}$$

The method of variation of parameters can now be employed to find the solution  $\hat{\zeta}(r, \theta; \omega)$  of the inhomogeneous equation of motion (2.6). We assume for  $\hat{\zeta}$  the same algebraic expression as  $\zeta_h$ , i.e.

$$\hat{\zeta}(r, \theta; \omega) = \sum_{n=0}^{\infty} G_n(r; \omega) \cos n\theta, \tag{2.13}$$

with  $G_n$  unknown functions. By using the expansion (2.13) into the inhomogeneous equation (2.6) and employing the orthogonality property

$$\int_{-\pi}^{\pi} \cos m\theta \cos n\theta d\theta = \frac{2\pi}{\epsilon_n} \delta_{nm},$$

$\epsilon_n$  being the Jacobi function and  $\delta_{nm}$  the Kronecker operator, an inhomogeneous ordinary differential equation for  $G_n(r; \omega)$  is obtained:

$$G_{n,rr} + \left( \frac{1}{r} + \frac{1}{r - r_0} \right) G_{n,r} + \left[ \frac{(i\omega)^2}{r - r_0} - \frac{n^2}{r^2} \right] G_n = -\frac{1}{r - r_0} F_n(r; \omega), \tag{2.14}$$

which is the CHE of complex parameter  $i\omega$  (2.8), forced by the function

$$F_n(r; \omega) = \frac{\epsilon_n}{2\pi} \int_{-\pi}^{\pi} \hat{f}_u(r, \theta; \omega) \cos n\theta d\theta. \tag{2.15}$$

For a translating Gaussian sea-floor movement with initial position of the landslide centroid  $r_s = r'_s/\sigma$ , the time-dependent perturbation of the sea floor is

$$f(r, \theta, t) = \exp \{ -[r - r_c(t)]^2 - (\gamma\theta)^2 \}, \tag{2.16}$$

where  $\gamma = 1/\theta_0$ ,  $\theta_0$  is the characteristic angle subtended by the landslide and  $r_c(t) = r_s + t$  the radial coordinate of the centroid, moving at the uniform speed  $u = 1$ . With reference to figure 2, if  $\lambda$  is the characteristic width of the landslide, then  $\gamma = 1/\theta_0 = r'_s/2\lambda$ . The forcing term  $F_n$ , expression (2.15), can be integrated twice by

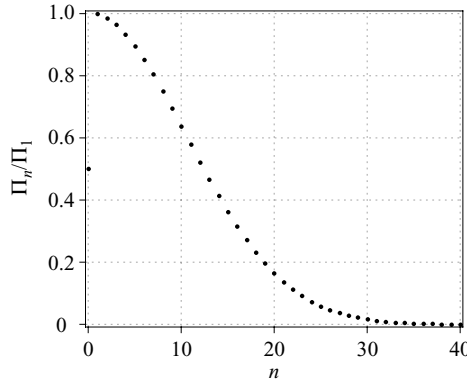


FIGURE 3. Behaviour of the ratio  $\Pi_n/\Pi_1$  with increasing modal order  $n$ . Parameters are  $\sigma = 0.175$  m,  $\lambda = \sigma/2$ ,  $r_s = 7.43$ ,  $\gamma = 7.43$ , modelling the geometry of the conical island of § 4.1.

parts, yielding

$$F_n(r; \omega) = \Pi_n \left\{ - [2(r - r_s) + \omega] e^{-(r-r_s)^2} + \omega^2 \frac{\sqrt{\pi}}{2} e^{-\omega(r-r_s) + \omega^2/4} \left[ 1 + \operatorname{erf} \left( r - r_s - \frac{\omega}{2} \right) \right] \right\}, \quad (2.17)$$

where

$$\Pi_n = \frac{\epsilon_n e^{-n^2/4\gamma^2}}{4\gamma\sqrt{\pi}} \left[ \operatorname{erf} \left( \gamma\pi + \frac{in}{2\gamma} \right) + \text{c.c.} \right], \quad (2.18)$$

c.c. being the complex conjugate.  $\Pi_n$  is a real amplitude factor dependent on the landslide characteristic angle  $1/\gamma$ ; figure 3 shows the fast decay of  $\Pi_n$  for increasing modal order  $n$ . The solution of the forced ordinary differential equation (2.14), subject to the boundary condition  $|G_n(r_0; \omega)| < \infty$ , is then

$$G_n(r; \omega) = \alpha_n Hc_n^{(1)}(r; i\omega) - P_n(r; \omega). \quad (2.19)$$

In (2.19)  $P_n$  is the particular solution

$$P_n(r; \omega) = \int_{r_0}^r \frac{F_n(\rho; \omega)}{(\rho - r_0) W(\rho)} \left[ Hc_n^{(1)}(\rho; i\omega) Hc_n^{(2)}(r; i\omega) - Hc_n^{(2)}(\rho; i\omega) Hc_n^{(1)}(r; i\omega) \right] d\rho. \quad (2.20)$$

$$W(r) = \frac{r_0}{r(r - r_0)}$$

is the Wronskian of the two homogeneous solutions  $Hc_n^{(1)}(r; i\omega)$  and  $Hc_n^{(2)}(r; i\omega)$  of the CHE (2.8), as shown in § A.2. By substituting (2.19) into the series expansion (2.13), the complete expression of the free-surface elevation transform in the near field is obtained

$$\hat{\zeta}(r, \theta; \omega) = \sum_{n=0}^{\infty} \left[ \alpha_n Hc_n^{(1)}(r; i\omega) - P_n(r; \omega) \right] \cos n\theta. \quad (2.21)$$

The integration constants  $\alpha_n$  in the above expression are to be determined by applying the matching conditions at the boundary  $r = b$ .



2.2.2. The far field  $r > b$

In the far field, the bottom depth is constant everywhere:  $h = h_b = b - r_0$ , and the direct influence of the forcing term on the behaviour of the fluid is negligible:  $f(r, \theta, t) \simeq 0$ . Then the governing equation (2.5) simplifies into

$$r^2 \hat{\xi}_{rr} + r \hat{\xi}_r - \frac{\omega^2 r^2}{h_b} \hat{\xi} + \hat{\xi}_{\theta\theta} = 0.$$

Separation of variables  $\hat{\xi}(r, \theta; \omega) = R(r; \omega)\Theta(\theta)$  yields the same angular solution as in the near field,  $\Theta_n = \cos n\theta$ ,  $n = 0, 1, 2, \dots$  while for the radial part  $R_n$

$$r^2 R_{n,rr} + r R_{n,r} - \left( \frac{\omega^2 r^2}{h_b} + n^2 \right) R_n = 0. \tag{2.22}$$

With the change of variables  $x = kr$ , with  $k = \omega/\sqrt{h_b}$ , (2.22) becomes a standard modified Bessel equation, whose independent solutions are the two modified Bessel functions  $I_n(x)$  and  $K_n(x)$ . The general solution of the governing equation (2.22)

$$R_n(r; \omega) = \alpha_n I_n \left( \frac{\omega r}{\sqrt{h_b}} \right) + \beta_n K_n \left( \frac{\omega r}{\sqrt{h_b}} \right)$$

has a branch-cut on the negative real axis of the complex plane  $\omega$  introduced by  $K_n$ . Note that, since  $\omega = c + id$  has a positive real part  $c$ ,  $\arg(\omega r/\sqrt{h_b}) \in (-\pi/2, \pi/2)$ . Now, for  $|\arg(x)| < \pi/2$  the modified Bessel function of first kind  $I_n(x) \simeq e^x/\sqrt{2\pi x}$  as  $|x| \rightarrow \infty$ . Hence, boundedness of the free-surface elevation as  $r \rightarrow \infty$  requires  $\alpha_n = 0$  and

$$R_n(r; \omega) = \beta_n K_n \left( \frac{\omega r}{\sqrt{h_b}} \right). \tag{2.23}$$

Finally, the free-surface elevation  $\hat{\xi}$  in the far field is

$$\hat{\xi}(r, \theta; \omega) = \sum_{n=0}^{\infty} R_n(r, \omega) \Theta_n(\theta) = \sum_{n=0}^{\infty} \beta_n K_n \left( \frac{\omega r}{\sqrt{h_b}} \right) \cos n\theta, \quad r > b. \tag{2.24}$$

The coefficients  $\beta_n$  in the above expression can be obtained by matching (2.24) with (2.21).

2.2.3. Matching

The near field solution (2.21) and the far field solution (2.24) are now matched at the common boundary  $r = b$ . Continuity of the free-surface elevation  $\hat{\xi}$  and the radial fluxes  $\hat{\xi}_r$  yields respectively for each  $n = 0, 1, 2, \dots$ ,

$$\begin{aligned} \alpha_n Hc_n^{(1)}(b; i\omega) - P_n(b; \omega) &= \beta_n K_n \left( \frac{\omega b}{\sqrt{h_b}} \right), \\ \alpha_n Hc_{n,r}^{(1)}(b; i\omega) - P_{n,r}(b; \omega) &= \beta_n K_{n,r} \left( \frac{\omega b}{\sqrt{h_b}} \right). \end{aligned}$$

The solution of the above inhomogeneous linear system is

$$\alpha_n(\omega) = \frac{1}{r_0} \int_{r_0}^b F_n(\rho; \omega) \rho \left[ Hc_n^{(1)}(\rho; i\omega) \frac{\Delta_n^{(2)}(\omega)}{\Delta_n^{(1)}(\omega)} - Hc_n^{(2)}(\rho; i\omega) \right] d\rho, \tag{2.25}$$

$$\beta_n(\omega) = \frac{1}{b h_b \Delta_n^{(1)}(\omega)} \int_{r_0}^b F_n(\rho; \omega) \rho Hc_n^{(1)}(\rho; i\omega) d\rho, \tag{2.26}$$

where

$$\Delta_n^{(1,2)}(\omega) = -Hc_n^{(1,2)}(b; i\omega) K_{n,r} \left( \frac{\omega b}{\sqrt{h_b}} \right) + K_n \left( \frac{\omega b}{\sqrt{h_b}} \right) Hc_{n,r}^{(1,2)}(b; i\omega). \quad (2.27)$$

The free-surface elevation transform in the complex half-plane  $|\arg(\omega)| < \pi/2$  is then

$$\hat{\zeta}(r, \theta; \omega) = \sum_{n=0}^{\infty} \left\{ \begin{array}{l} \alpha_n Hc_n^{(1)}(r; i\omega) - P_n(r; \omega) \\ \beta_n K_n \left( \frac{\omega r}{\sqrt{h_b}} \right) \end{array} \right\} \cos n\theta \quad \text{if } \left\{ \begin{array}{l} r_0 < r < b \\ r > b \end{array} \right\} \quad (2.28)$$

for the near field and the far field respectively, with  $\alpha_n$  and  $\beta_n$  given by (2.25) and (2.26) respectively.

### 3. Physical description

Inverse transform of (2.28) can be obtained by means of complex analysis. For the sake of clarity we shall first consider the free-surface elevation in the far field  $r > b$ .

#### 3.1. The far field

Inverse transform of (2.28) yields

$$\zeta(r, \theta, t) = \frac{1}{2\pi i} \sum_{n=0}^{\infty} \int_{c-i\infty}^{c+i\infty} \beta_n(\omega) K_n \left( \frac{\omega r}{\sqrt{h_b}} \right) e^{\omega t} d\omega \cos n\theta.$$

Upon substitution of (2.26) for  $\beta_n$ , the latter expression becomes

$$\zeta(r, \theta, t) = \sum_{n=0}^{\infty} \frac{1}{2\pi i b h_b} \int_{r_0}^b \rho \int_{c-i\infty}^{c+i\infty} f_n(\omega) e^{\omega t} d\omega d\rho \cos n\theta, \quad (3.1)$$

having defined

$$f_n(\omega) = \frac{F_n(\rho; \omega) Hc_n^{(1)}(\rho; i\omega) K_n(\omega r / \sqrt{h_b})}{\Delta_n^{(1)}(\omega)}, \quad (3.2)$$

where  $\rho \in (r_0, b)$  and  $r \in (b, \infty)$  are regarded as parameters, the forcing function  $F_n$  is given by (2.17) and the denominator  $\Delta_n^{(1)}$  by (2.27). Now, let us evaluate the inner integral of expression (3.1).

For  $t < 0$ , contour integration in the complex plane and usage of the asymptotic expressions of the confluent Heun functions (2.9) and (2.10) (see Appendix A.3) yield simply

$$\int_{c-i\infty}^{c+i\infty} f_n(\omega) e^{\omega t} d\omega = 0,$$

as shown in Appendix B.1. As a consequence,  $\zeta(r, \theta, t) = 0$  for  $t < 0$ .

For  $t > 0$ , contour integration in the complex plane gives

$$\int_{c-i\infty}^{c+i\infty} f_n(\omega) e^{\omega t} d\omega = i \int_{-\infty}^{+\infty} f_n(is) e^{ist} ds \quad (3.3)$$

as shown by some lengthy algebra in Appendix B.1. Now, substituting the latter result into (3.1), writing back the integrand in terms of  $\beta_n$  by using (3.2) and (2.26), and further transforming  $s = -\omega$ , yield

$$\zeta(r, \theta, t) = \sum_{n=0}^{\infty} \cos n\theta \frac{1}{2\pi} \int_{-\infty}^{\infty} \beta_n(-i\omega) K_n \left( \frac{-i\omega r}{\sqrt{h_b}} \right) e^{-i\omega t} d\omega \quad (3.4)$$

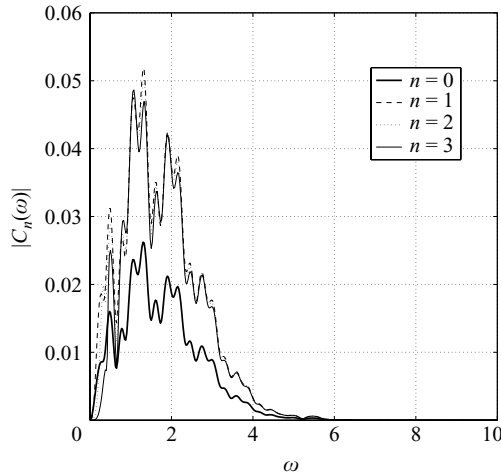


FIGURE 4. Plots of  $|C_n|$  versus  $\omega$ ; 25 Gauss points are needed for (3.6) to converge. Non-dimensional parameters are  $r_0 = 11.83$ ,  $r_s = \gamma = 7.43$  modelling the conical island of § 4.1.

for the free-surface elevation in the far field. Recalling that

$$K_n(x) = \frac{\pi}{2} i^{n+1} H_n(ix), \quad -\pi < \arg(x) \leq \pi/2,$$

where  $H_n$  is the Hankel function of first kind and order  $n$ , the free-surface elevation (3.4) in the far field  $r > b$  assumes the form

$$\zeta(r, \theta, t) = \sum_{n=0}^{\infty} \cos n\theta \int_{-\infty}^{\infty} C_n(\omega) H_n\left(\frac{\omega r}{\sqrt{h_b}}\right) e^{-i\omega t} d\omega, \quad (3.5)$$

having defined

$$C_n(\omega) = \frac{i^{n+1}}{4} \beta_n(-i\omega) = \frac{1}{4bh_b} \frac{i^{n+1}}{\Delta_n^{(1)}(-i\omega)} \int_{r_0}^b \rho F_n(\rho; -i\omega) Hc_n^{(1)}(\rho; \omega) d\rho. \quad (3.6)$$

Let us further introduce the symbol  $()^*$  to denote the complex conjugate of  $()$ . Then from (3.6) it is straightforward to show that the integrand of (3.5) satisfies the property

$$C_n(-\omega) H_n\left(\frac{-\omega r}{\sqrt{h_b}}\right) e^{i\omega t} = C_n^*(\omega) H_n^*\left(\frac{\omega r}{\sqrt{h_b}}\right) (e^{-i\omega t})^*.$$

As a consequence, the free-surface elevation (3.5) becomes

$$\zeta(r, \theta, t) = \sum_{n=0}^{\infty} \cos n\theta \int_0^{\infty} C_n(\omega) H_n\left(\frac{\omega r}{\sqrt{h_b}}\right) e^{-i\omega t} d\omega + \text{c.c.}, \quad (3.7)$$

i.e. a real number. Integrals like (3.6) on the finite domain  $(r_0, b)$  can be conveniently evaluated via the Gauss–Legendre quadrature method (see Press *et al.* 1986, for details). Numerical evaluation of (3.6) shows that the  $|C_n(\omega)|$  fast decay with increasing  $\omega$ , as depicted in figure 4; as a result the convergence of the integral (3.7) is assured. Now define  $k = \omega/\sqrt{h_b}$  the wavenumber in the far field. Then note that each spectral component of the free-surface elevation (3.7) is proportional to  $H_n(kr)e^{-i\omega t}$ , i.e. outgoing in the far field. This result agrees with the general theory of Longuet-Higgins (1967), Meyer (1971) and Summerfield (1971) already discussed in § 1. Note

also that  $\zeta(r, \theta, t)$  (3.7) is obtained by integrating the frequency response  $H_n(kr)$  to an incident wavetrain of unit amplitude, multiplied by the forcing factor  $C_n(\omega)$ . This solution is similar to many other linear-system responses to transient excitations, like for example the harbour response to a transient incident wave (see Mei *et al.* 2005).

### 3.2. The leading wave

As anticipated in § 1, the transient landslide-generated disturbance propagating around the island is not perfectly trapped. In this section we investigate on the existence of a leading wave propagating radially at large distances from the coastline,  $r \gg 1$ . Let us consider the free-surface elevation (3.7); to obtain an approximate expression of  $\zeta$  at large distances from the island, use the asymptotic expansion of the Hankel function for large argument

$$H_n(x) \simeq \sqrt{\frac{2}{\pi x}} e^{i(x - \pi n/2 - \pi/4)},$$

so that

$$\zeta(r, \theta, t) \simeq \sum_{n=0}^{\infty} \cos n\theta e^{-i(\frac{\pi n}{2} + \frac{\pi}{4})} \int_0^{\infty} C_n(\omega) \sqrt{\frac{2\sqrt{h_b}}{\pi\omega r}} e^{i\omega(r/\sqrt{h_b} - t)} d\omega + \text{c.c.} \quad (3.8)$$

Since the wavefront moves at the group celerity  $C_g = d\omega/dk = \sqrt{h_b}$ , its position at a given time is described by  $r = \sqrt{h_b}t$ . Substitution of the latter relation inside (3.8), yields the expression of the leading wave  $\zeta_l(\theta, t)$

$$\zeta_l(\theta, t) \simeq \sqrt{\frac{2}{\pi t}} \sum_{n=0}^{\infty} \mathcal{A}_n \cos n\theta, \quad (3.9)$$

where the real values

$$\mathcal{A}_n = e^{-i(\frac{\pi n}{2} + \frac{\pi}{4})} \int_0^{\infty} \frac{C_n(\omega)}{\sqrt{\omega}} d\omega + \text{c.c.} \quad (3.10)$$

are modal amplitudes. The latter integral on the infinite domain  $(0, \infty)$  can be evaluated by employing the more advanced Gauss–Kronrod iterative method. Note that the leading wave (3.9) decays as  $O(t^{-1/2})$  in the three-dimensional geometry of the shelf, i.e. it vanishes faster than the leading Airy wave,  $O(t^{-1/3})$ , generated by a transient disturbance in a two-dimensional ocean of constant depth (see Mei *et al.* 2005).

Let us now investigate on the influence of the distinctive parameters of the system,  $b'$  (bottom radius) and  $\sigma$  (characteristic length of the slide), upon the characteristics of the leading wave travelling offshore. The amplitude  $\mathcal{A}_n$  of the  $n$ th leading wave component (3.10) depends on  $C_n$  (3.6), which in turn is a function of the ratio  $b = b'/\sigma$ . As shown in figure 5, the  $\mathcal{A}_n$  fast decay as  $b$  increases. Physically, the submerged beach surrounding the island acts as a barrier to trap wave energy: the longer the beach with respect to the slide, the less the energy propagated offshore. We now turn to the analysis of the near field and the free-surface runoff.

### 3.3. The near field

In the near field  $r < b$  inverse transform of (2.28) yields

$$\zeta(r, \theta, t) = \frac{1}{2\pi i} \sum_{n=0}^{\infty} \int_{c-i\infty}^{c+i\infty} [\alpha_n(\omega) Hc_n^{(1)}(r/r_0; i\omega) - P_n(r; \omega)] e^{\omega t} d\omega \cos n\theta.$$

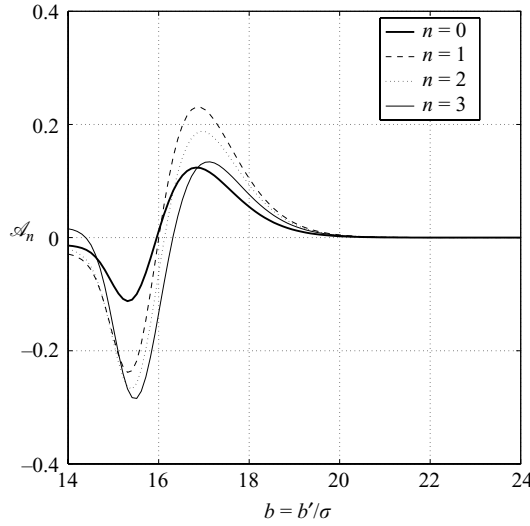


FIGURE 5. Plots of  $\mathcal{A}_n$  versus  $b = b'/\sigma$ , evaluated with the Gauss–Kronrod quadrature method. Non-dimensional parameters are  $r_0 = 11.83$ ,  $r_s = \gamma = 7.43$ , modelling the conical island of §4.1. Note that the  $\mathcal{A}_n$  fast decay by increasing  $b$ .

By using (2.25) for  $\alpha_n$  and (2.20) for the particular solution  $P_n$ , the free-surface elevation can be expressed as

$$\zeta(r, \theta, t) = \frac{1}{2\pi i r_0} \sum_{n=0}^{\infty} \cos n\theta \left[ \int_{r_0}^b \rho \int_{c-i\infty}^{c+i\infty} f_{1n}(\rho, \omega) e^{\omega t} d\omega d\rho - \int_{r_0}^r \rho \int_{c-i\infty}^{c+i\infty} f_{2n}(\rho, \omega) e^{\omega t} d\omega d\rho \right]. \quad (3.11)$$

In (3.11) the two integrand functions are

$$f_{1n}(\rho, \omega) = F_n(\rho; \omega) \left[ Hc_n^{(1)}(\rho; i\omega) \frac{\Delta_n^{(2)}(\omega)}{\Delta_n^{(1)}(\omega)} - Hc_n^{(2)}(\rho; i\omega) \right] Hc_n^{(1)}(r; i\omega) \quad (3.12)$$

and

$$f_{2n}(\rho, \omega) = F_n(\rho; \omega) \left[ Hc_n^{(1)}(\rho; i\omega) Hc_n^{(2)}(r; i\omega) - Hc_n^{(2)}(\rho; i\omega) Hc_n^{(1)}(r; i\omega) \right] \quad (3.13)$$

respectively. In the latter expressions,  $F_n$  is the forcing function (2.17), while  $\Delta_n^{(1,2)}$  are given by (2.27). In order to solve (3.11), consider the contour integrals

$$\int_{c-i\infty}^{c+i\infty} f_{jn}(\rho, \omega) d\omega, \quad j = 1, 2 \quad (3.14)$$

and employ again the technique used to get the inverse transform of  $\zeta$  in the far field.

For  $t < 0$ , as shown in Appendix B.2, it is straightforward to show

$$\int_{c-i\infty}^{c+i\infty} f_{jn}(\rho, \omega) d\omega = 0, \quad j = 1, 2$$

implying  $\zeta(r, \theta, t) = 0$ .

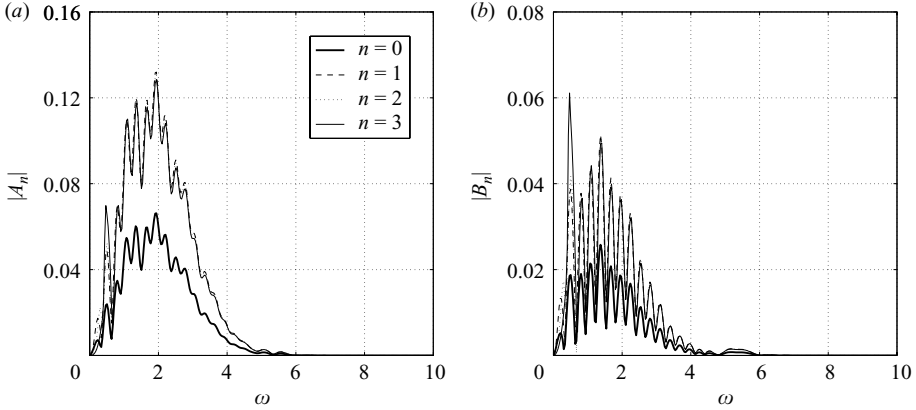


FIGURE 6. Plots of  $|A_n|$  (a) and  $|B_n|$  (b) versus  $\omega$  at  $r = 15$ . Non-dimensional parameters are  $r_0 = 11.83$ ,  $r_s = \gamma = 7.43$ , modelling the conical island of § 4.1.

For  $t > 0$  contour integration in the complex plane yields

$$\int_{c-i\infty}^{c+i\infty} f_{jn} e^{\omega t} d\omega = i \int_{-\infty}^{+\infty} f_{jn}(is) e^{ist} ds, \quad j = 1, 2, \quad (3.15)$$

as shown in Appendix B.2. Substituting (3.15) back into (3.11) and further transforming  $s = -\omega$ , we obtain

$$\begin{aligned} \zeta(r, \theta, t) = \frac{1}{2\pi r_0} \sum_{n=0}^{\infty} \cos n\theta \left[ \int_{r_0}^b \rho \int_{-\infty}^{\infty} f_{1n}(\rho, -i\omega) e^{-i\omega t} d\omega d\rho \right. \\ \left. - \int_{r_0}^r \rho \int_{-\infty}^{\infty} f_{2n}(\rho, -i\omega) e^{-i\omega t} d\omega d\rho \right]. \quad (3.16) \end{aligned}$$

By making use of both definitions (3.12) and (3.13) for the  $f_{jn}$ , the free-surface elevation in the near field (3.11) can be finally expressed as

$$\zeta(r, \theta, t) = \sum_{n=0}^{\infty} \cos n\theta \int_0^{+\infty} [A_n(r; \omega) Hc_n^{(1)}(r; \omega) + B_n(r; \omega) Hc_n^{(2)}(r; \omega)] e^{-i\omega t} d\omega + c.c., \quad (3.17)$$

where

$$\begin{aligned} A_n(r; \omega) = \frac{1}{2\pi r_0} \int_{r_0}^b \rho F_n(\rho; -i\omega) \left[ Hc_n^{(1)}(\rho; \omega) \frac{\Delta_n^{(2)}(-i\omega)}{\Delta_n^{(1)}(-i\omega)} - Hc_n^{(2)}(\rho; \omega) \right] \\ + \frac{1}{2\pi r_0} \int_{r_0}^r \rho F_n(\rho; -i\omega) Hc_n^{(2)}(\rho; \omega) d\rho \quad (3.18) \end{aligned}$$

and

$$B_n(r; \omega) = -\frac{1}{2\pi r_0} \int_{r_0}^r \rho F_n(\rho; -i\omega) Hc_n^{(1)}(\rho; \omega) d\rho, \quad (3.19)$$

being  $A_n(r; -\omega) = A_n^*(r; \omega)$  and  $B_n(r; -\omega) = B_n^*(r; \omega)$ . As shown in figure 6, the terms  $|A_n|$  and  $|B_n|$  are fast-decaying oscillating functions of  $\omega$ , so that the integral in (3.17) is convergent. Finally, note that in the limit  $r \rightarrow b$ , the expressions of the free-surface elevation respectively in the near field (3.17) and in the far field (3.7)

coincide. The solution (3.17) in the near field is a transient propagating wave. It is obtained by summing over the positive real frequency spectrum the two independent solutions  $Hc_n^{(1)}$  and  $Hc_n^{(2)}$  of the governing equation (2.8), multiplied by the forcing factors  $A_n$  and  $B_n$  respectively. The free-surface elevation in the far field (3.7) and in the near field (3.17) can be evaluated by solving numerically the relevant integral expressions over the infinite domain  $\omega \in (0, \infty)$ ; fast-converging method such as the Gauss–Kronrod quadrature can be employed with reliable accuracy.

### 3.4. The free-surface runup

The runup at the shoreline is a variable of interest for risk assessment purposes. Substitution of  $r = r_0$  into the free-surface elevation  $\zeta$ , expression (3.17), determines the second integral in (3.18) and the  $B_n$ s to be null. The corresponding value of the free-surface runup is therefore

$$\zeta(r_0, \theta, t) = \sum_{n=0}^{\infty} \cos n\theta \int_0^{+\infty} A_n(r_0, \omega) e^{-i\omega t} d\omega + \text{c.c.}, \tag{3.20}$$

where

$$A_n(r_0, \omega) = \frac{1}{2\pi r_0} \int_{r_0}^b \rho F_n(\rho, -i\omega) \left[ Hc_n^{(1)}(\rho; \omega) \frac{\Delta_n^{(2)}(-i\omega)}{\Delta_n^{(1)}(-i\omega)} - Hc_n^{(2)}(\rho; \omega) \right] d\rho. \tag{3.21}$$

In (3.21)  $\Delta_n^{(1,2)}$  are still given by (2.27), while  $F_n$  is again the forcing function defined by (2.17). In §4, parametric discussion of the free-surface runup is made; the physical observations on the free-surface runup, heights and periods made by Di Risio *et al.* (2009*b*) are compared with numerical integration of expression (3.20). Finally, discussion is made on the mean features of the solution, pointing out the differences between tsunamis propagating around a conical island and tsunamis propagating along a plane beach.

## 4. Discussion

### 4.1. Experimental comparison

In order to validate the theory, comparison is made with the experimental results of Di Risio *et al.* (2009*b*). The dimensions of the basin, the island and the landslide used in the experiments, are indicated in table 1. The initial position of the landslide centroid,  $r'_s = 1.3$  m, is such that the mass at the starting position rests completely out of the water, thus representing a subaerial slide. The mass, reproducing half of an ellipsoid, is a rigid block with flat bottom, sliding along a plane slope 0.5 m wide, as shown in figure 7. The resulting geometry is that of a plane slope connected to the curved flanks of a conical island, i.e. slightly different from the conical island of the analytical model. Note also that the landslide used in the experiments preserves its shape during all the phases of motion. On the other hand, the landslide described analytically by (2.16) modifies its shape adapting to the curvature of the island while sliding along its flanks. As a result, the theoretical volume of the slide

$$\begin{aligned} V'(t) &= \sigma^2 H \int_{-\pi}^{\pi} \int_0^{\infty} f(r, \theta, t) r dr d\theta \\ &= \frac{\sqrt{\pi}}{2} \frac{\sigma^2 H \text{Herf}(\gamma\pi)}{\gamma} \{ e^{-(r_s-t)^2} + \sqrt{\pi} [\text{erf}(r_s + t) + 1] (r_s + t) \} \end{aligned} \tag{4.1}$$

<b>Basin</b>			
Length (m)	Width (m)	Depth (m)	
50.00	30.00	3.00	
<b>Island</b>			
Wet contour $r'_0$ (m)	Bottom radius $b'$ (m)	Flank slope $s$	
2.07	4.45	1/3	
<b>Landslide</b>			
Length (m)	Width (m)	Max vert. height $H$ (m)	Initial position $r'_s$ (m)
0.80	0.40	0.045	1.3

TABLE 1. Basin, island and landslide dimensions of the laboratory experiment made by Di Rasio *et al.* (2009b).

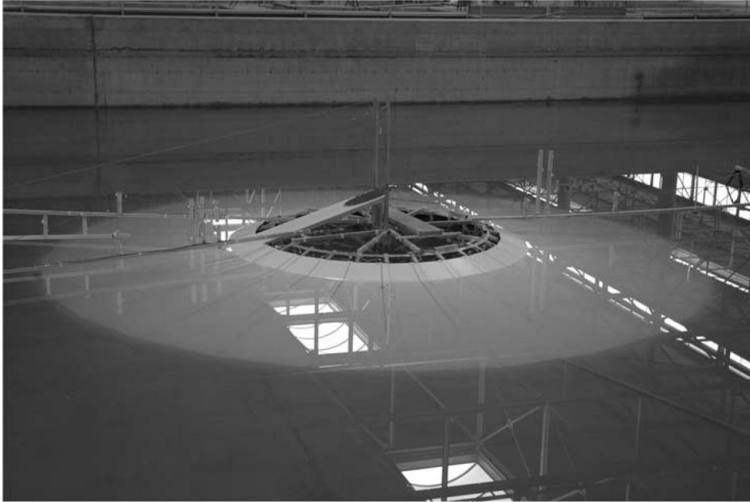


FIGURE 7. View of the experimental device used by Di Rasio *et al.* (2009b). The landslide is forced to move along a plane incline 0.5 m wide; as a result the geometry of the experimental model is that of a very thin plane-beach strip connected to the curved flanks of a conical island.

depends on time, increasing linearly for large  $t$ . This curvature-induced increase of volume, even if physically reasonable, is absent in the experimental model, therefore the equivalence in volume of the analytical and the experimental slides cannot be strictly applied. However mean quantities can still be represented. We choose the characteristic parameters  $\sigma = 0.175$  m and  $\lambda = \sigma/2$  to match respectively the wave period time scale in the experiments  $T'(\propto \sqrt{\sigma/gs}) \simeq 2$  s and the shape of the landslide, whose characteristic width to length ratio is  $\lambda : \sigma = 1 : 2$ . With this choice, the volume of the theoretical landslide at the beginning of motion is  $V'(0) = 0.0045$  m<sup>3</sup> and then increases linearly, equating the volume of the experimental slide  $V'_{exp} = 0.0084$  m<sup>3</sup> at about  $t' \simeq 1.6$  s, as shown in figure 8. At larger times  $V' > V'_{exp}$  and still increasing,



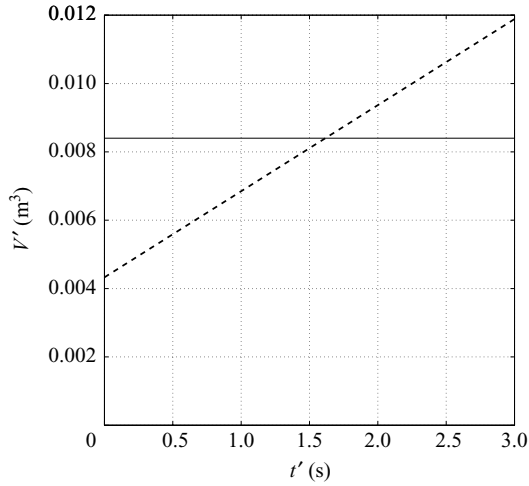


FIGURE 8. Volume of the analytical landslide (bold dashed line) evaluated with (4.1) and of the experimental landslide (continuous line) versus time. The first one increases almost linearly with time while the landslide moves along the flanks of the island; the second one is constant during all the phases of motion.

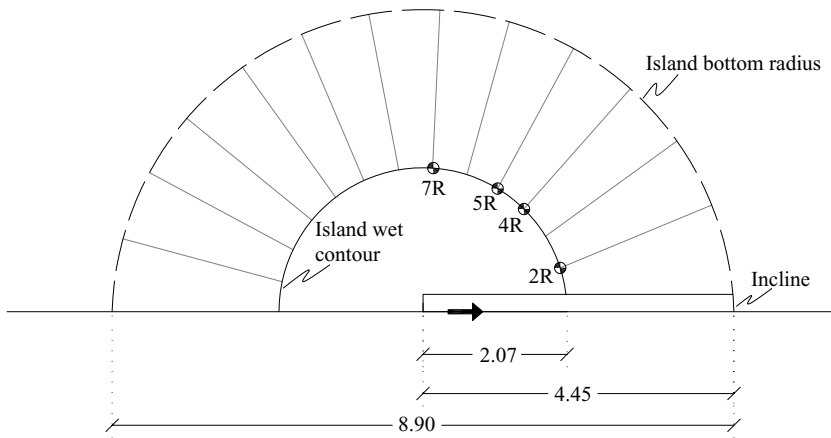


FIGURE 9. Sketch of half of the conical island with the positions of the sample points considered for experimental comparison and indication of the island dimensions (in metres). The solid line (—) represents the island wet contour  $r'_0$ , while the island bottom radius  $b'$  is indicated by the dashed line (---). The bold arrow indicates the direction of motion of the sliding mass. Segments on the island flanks indicate the position of the gauges employed in the experiments of Di Risio *et al.* (2009b).

but the slide approaches deeper water and its influence on the generated wave field can be neglected.

The sample points along the shoreline 2R(20.6°), 4R(47.6°), 5R(60.2°) and 7R(86.3°) ('R' stands for runup) of Di Risio *et al.* (2009b), sketched in figure 9, have been chosen for comparison. In figure 10(a–d), the time series of the free-surface runup, expression (3.20), are plotted in physical variables at the chosen sample points (see figure 9) and compared to the experimental time series of Di Risio *et al.* (2009b). Figure 10(a) shows the time series of the free-surface runup at  $\theta = 20.6^\circ$  (gauge 2R), i.e. about

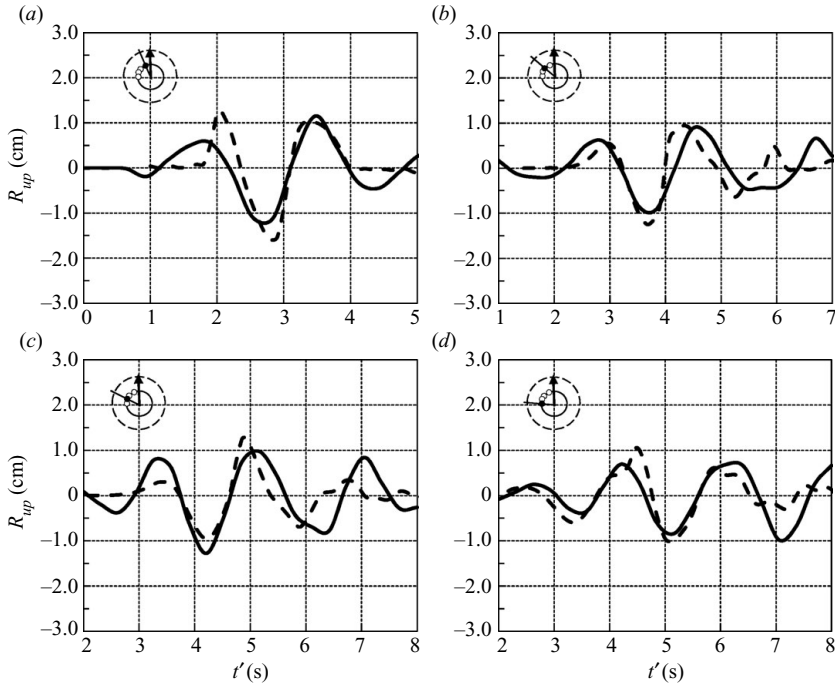


FIGURE 10. Analytical (bold line) and experimental (bold dashed line) time series of the free-surface runup  $R_{up} = \zeta'(r'_0, \theta, t')$  at the shoreline in physical variables. The geometry of the island and the landslide is reported in table 1. The Gauss–Kronrod quadrature method has been used for numerical integration of (3.20), modes  $n = 0 \dots 10$  have been taken into account. Subplot (a) refers to the shoreline point 2R located at  $\theta = 20.6^\circ$ , subplot (b) refers to 4R located at  $\theta = 47.6^\circ$ , subplot (c) to 5R located at  $\theta = 60.2^\circ$  and subplot (d) to 7R located at  $\theta = 86.3^\circ$ . In each of the subplots, a plant view of the island is sketched on the top left corner. Here, the solid line (—) represents the island wet contour, while the dashed line (---) represents the island bottom radius. The arrow indicates where the slide enters the water and the filled circle specifies the position of the relevant runup gauge.

0.72 m ( $\simeq 4\sigma$ ) from the point of tsunami generation. In figure 10(b) is instead depicted the time series of the free-surface runup at  $\theta = 47.6^\circ$  (gauge 4R), i.e. about 1.24 m ( $\simeq 7\sigma$ ) far from the origin. Figure 10(c) shows the runup time series at  $\theta = 60.2^\circ$  (gauge 5R), i.e. about 2.17 m ( $\simeq 12\sigma$ ) far from the origin and finally in figure 10(d) is depicted the runup time series at  $\theta = 86.3^\circ$  (gauge 7R), i.e. about 3.12 m ( $\simeq 18\sigma$ ) from the point of tsunami generation. Overall, the graphs show good correspondence between the analytical results and the experimental ones. The main properties of the generated wave field, i.e. the shape of the waves, the time of arrival of crests and troughs and the maximum runup and drawdown, are predicted satisfactorily by the analytical model. Other than the difference in landslide volumes pointed up above, several minor factors can also explain the slight differences between the analytical and the experimental data. Firstly, recall that the geometry of the experimental model is a narrow plane beach surrounded by a conical island. The presence of this thin-strip plane beach influences the overall behaviour of the fluid in the neighbourhood of the generation zone. Due to the energy-trapping property of the straight coast, the maximum runup obtained in the experiment is larger than the one obtained with the analytical model for a purely conical island (which is unable to trap energy completely) especially near the generation zone (see point 2R in figure 10a). Secondly,

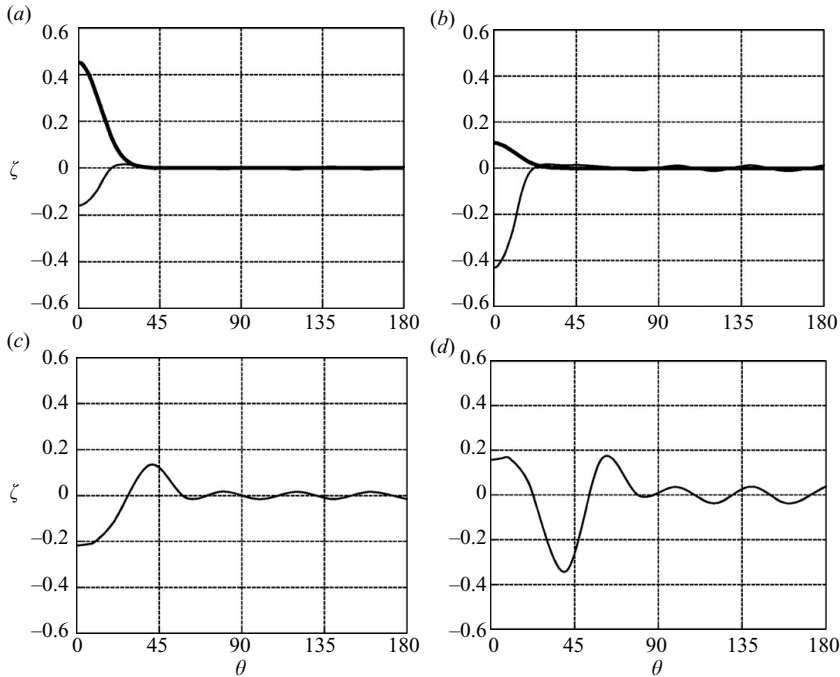


FIGURE 11. Spatial snapshots of the free-surface elevation in non-dimensional variables for a subaerial landslide at the shoreline.  $\theta$  in degrees. The dimensions of the island are those of table 1, the slide characteristic length is  $\sigma = 0.37$  m,  $\lambda = \sigma/2$ . The centroid initial position is  $r_s = 3.51$  ( $r'_s = 1.3$  m). Bold lines depict the landslide surface contour  $f(r_0, \theta, t)$  at the given times, solid lines represent the free-surface elevation  $\zeta(r_0, \theta, t)$ . Subplot (a) refers to  $t = 2.97$  ( $t' = 1$  s), subplot (b) refers to  $t = 3.57$  ( $t' = 1.2$  s), subplot (c) to  $t = 5.94$  ( $t' = 2$  s) and finally subplot (d) refers to  $t = 8.92$  ( $t' = 3$  s). Modes  $n = 0-9$  have been considered. Note that the symmetry condition  $\partial\zeta/\partial\theta = 0$  at  $\theta = 0$  is fully reproduced by the model.

note that the long-wave governing equation (1.1) used in the model is non-dispersive, hence the dispersive behaviour of water waves on a bottom with varying depth cannot be properly rendered with the analytical model used here. As a result, while in the experimental time series the period of the first incoming waves is longer than that of the following group, in the analytical model the wave period is almost constant for all the waves in the group (see figure 10*b,c*). Finally, note that the landslide used in the experiments is not of a double Gaussian shape, but is an half an ellipsoid. The difference in the front shape, which in the model is much smoother than in the experiments, could have led to some diversities in the shape of the first propagating waves.

#### 4.2. Tsunami generation and propagation around the island

After having shown a good agreement between the theoretical and the experimental data, we analyse the tsunami generation and propagation mechanisms more in detail. In figure 11(*a-d*) snapshots of the non-dimensional free-surface runup  $\zeta(r_0, \theta, t)$  at four different times are shown, together with the contour of the slide  $f(r_0, \theta, t)$ . The geometry of the island is still that of table 1. The landslide is kept subaerial ( $r'_s = 1.3$  m), but its characteristic length is increased to  $\sigma = 0.37$  m ( $r_s = r'_s/\sigma = 3.51$ ), still being  $\lambda = \sigma/2$ . The larger ratio  $\sigma/b'$  allows to gain a clearer insight on the early interaction between the slide and the water occurring during the generation process.

At the first instants of motion (figure 11*a, b*) the shoreline recedes as the landslide pushes water away. The early depression wave formed landwards of the slide is clearly a source-related perturbation, having the same width as that of the slide (Lynett & Liu 2005, found numerically a similar result for landslide tsunamis along a plane beach). Moving ahead in time, the slide disappears in deeper water (figure 11*c, d*). At the origin the shoreline inverts its motion and goes back up the incline (figure 11*c*), due to the elastic rebound. The perturbation leaves the origin with the profile of a positive N-wave along the coastline, as shown in figure 11*c*). Finally, water inundates the dry land at the origin (figure 11*d*), meanwhile the leading elevation wave is travelling around the island, followed by a deeper trough. Note that the generation mechanisms of landslide tsunamis around a conical island do not differ from those of landslide tsunamis along a plane beach (see Lynett & Liu 2005; Sammarco & Renzi 2008). In fact, the shoreline snapshots of figure 11(*a–d*) resemble very closely the digital pictures of the shoreline position taken by Di Risio *et al.* (2009*a*) during the experimental modelling of landslide tsunamis along a plane beach. At larger times, however, the smaller refractive power of the island enhances the amount of energy radiated to infinity. As a result, the wave field propagating around the island differs from the one propagating along the plane beach, as shown in the following section.

#### 4.3. *The conical island versus the plane beach*

In this section, the features of tsunamis propagating around a conical island are further compared to the features of landslide-generated tsunamis on a plane beach (see Sammarco & Renzi 2008). To perform this comparison, beach slope and landslide characteristic parameters are kept equal, i.e.  $s = 1/3$ ,  $\sigma = 0.37$  m,  $\lambda = \sigma/2$  in both geometries; landslide is half-submerged in its initial position in both cases. The island geometry is the same of table 1, the half-submergence condition requires the landslide centroid position at  $r'_s = r'_0 = 2.07$  m. Figures 12(*a*) and 12(*b*) show the time series of the free-surface runup (expression 3.20) in non-dimensional variables at the shoreline points  $1S = (r_0, 20.6^\circ)$  and  $2S = (r_0, 60.2^\circ)$  respectively, while figures 12(*c*) and 12(*d*) show the free-surface elevation time series in the far field (expression 3.7) at the offshore points  $1O = (b, 0^\circ)$  and  $2O = (2b, 0^\circ)$  respectively. As the landslide motion begins, water is pushed ahead and a leading elevation wave travelling offshore is generated, quickly reaching the two points  $1O$  at  $r = b$  (figure 12*c*) and  $2O$  at  $r = 2b$  (figure 12*d*) in the far field. Note also the strong attenuation experienced by the leading wave crest while travelling from point  $1O$  to point  $2O$ . In the meantime, a deep depression wave occurs just behind the slide. As a result, at point  $1S$  on the shoreline close to the origin the first incoming wave has a trough, followed by a large crest generated by the elastic rebound (see figure 12*a*). The maximum runup is reached by the first crest, then oscillations decay in time, the free-surface elevation eventually reaching the unperturbed position. At point  $2S$  on the shore far from the origin the first wave has instead a small crest, followed by a larger trough (see figure 12*b*), i.e. the first incoming perturbation is still a positive N-wave. Note that the maximum runup here is reached by the second incoming wave, which is followed in turn by a tail of smaller-amplitude waves. The fact that at large distances from the slide the largest wave is shifted towards the middle of the group is also a feature of tsunamis propagating along a plane beach. As demonstrated numerically by Lynett & Liu (2005), experimentally by Di Risio *et al.* (2009*a*) and then analytically by Sammarco & Renzi (2008), this characteristic is due to the excitation of edge-wave modes trapped along the straight coast. The occurrence of such a phenomenon around the shoreline of the conical island suggests that edge-wave components of

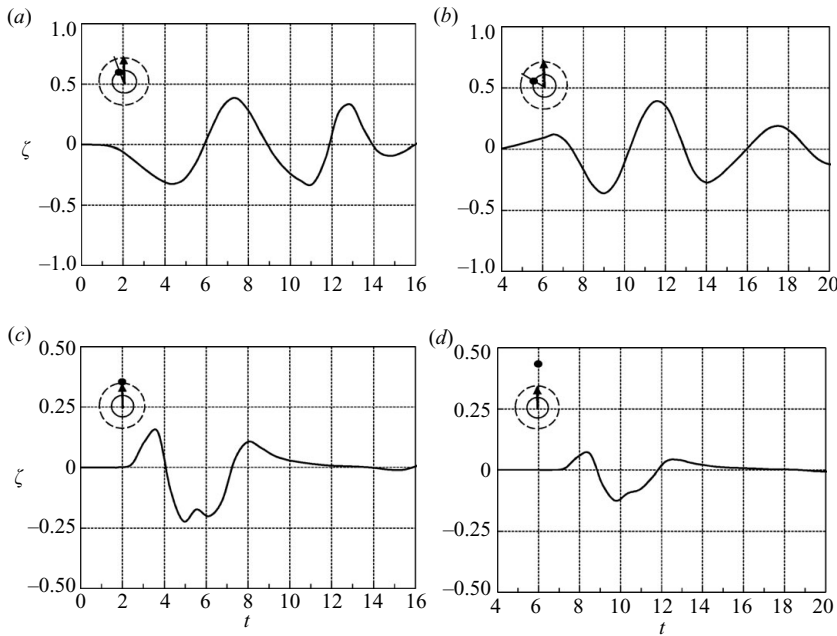


FIGURE 12. Time series in non-dimensional variables for a half-submerged landslide ( $r_s = r_0$ ). Subplot (a) refers to the shoreline point  $1S$  located at  $(r_0, \theta = 20.6^\circ)$ , subplot (b) refers to  $2S$  at  $(r_0, \theta = 60.2^\circ)$ , subplot (c) to the far-field point  $1O$  at  $(b, 0^\circ)$  and finally subplot (d) refers to point  $2O$  at  $(2b, 0^\circ)$ . Modes  $n = 0-9$  have been considered. In each of the subplots, a plan view of the island is sketched on the top left corner. Here, the solid line (—) represents the island wet contour, while the dashed line (---) represents the island bottom radius. The arrow indicates where the slide enters the water and the filled circle specifies the position of the relevant point.

the water motion can be partially trapped along the coast also in a round geometry. Let us demonstrate this feature analytically by looking at expression (3.20) for the runup  $\zeta(r_0, \theta, t)$ . This is obtained for each of the angular modal components by integrating with respect to  $\omega \in \mathbb{R}$  the form  $e^{-i\omega t}$ , representing a simple harmonic oscillation in time, multiplied by the forcing factor  $A_n(r_0, \omega)$ , expression (3.21). The latter physically represents the amplitude of each wave component in the frequency domain. Figure 13 shows the fast decay of  $|A_n(r_0, \omega)|$  for increasing  $\omega$ , so that the effective domain of integration of (3.20) is restricted only to smaller  $\omega$ , for each of the angular modal components. Therefore only the lowest frequencies concur in determining the magnitude of the free-surface runup at the shoreline. Now, recalling condition (1.4), the lowest frequencies experience the strongest exponential attenuation as  $r$  increases towards infinity (see also Meyer 1971; Mei *et al.* 2005): the relevant wave components are almost trapped around the shoreline, resembling the edge-wave modes. Hence the free-surface runup, expression (3.20), can be regarded almost as a sum of edge-wave-like modes, for which the largest wave is always shifted towards the middle of the group (see Sammarco & Renzi 2008).

Are then any practical differences between the wave fields generated around a conical island and along a plane beach? A direct comparison of the relevant runup time series shows them. The bold dashed lines in figure 14(a,b) show the free-surface runup time series at points  $y' = 0.72$  m ( $y = y'/\sigma = 2.05$ , corresponding to  $1S$ ) and  $y' = 2.175$  m ( $y = y'/\sigma = 5.88$ , corresponding to  $2S$ ) along the shoreline of a plane

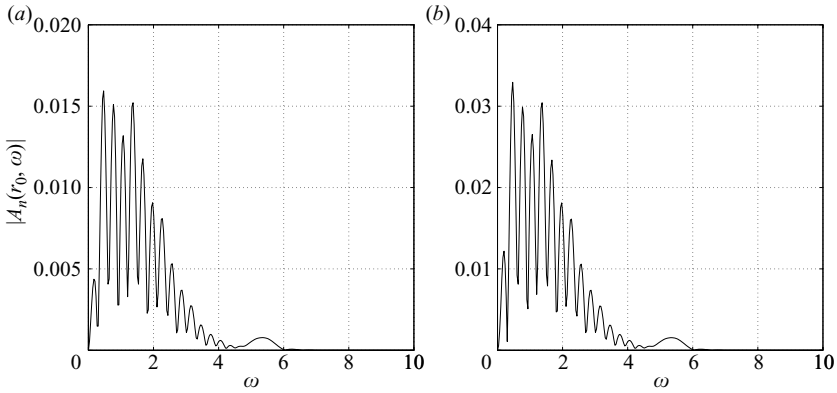


FIGURE 13. Plots of  $|A_n(r_0, \omega)|$  versus frequency  $\omega$  for the geometry used in the experiments of Di Risio *et al.* (2009b). Modal orders are (a)  $n=0$ , (b)  $n=1$ .

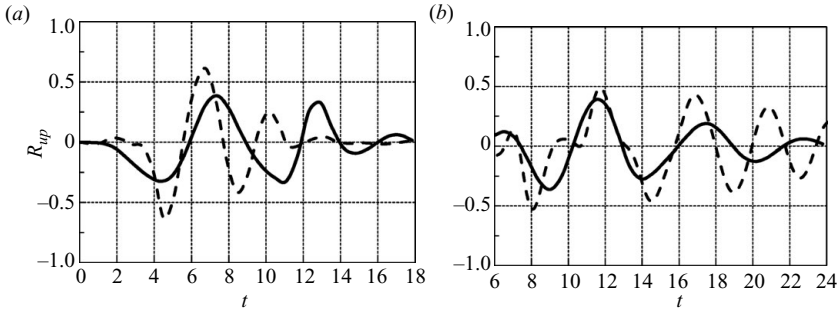


FIGURE 14. Free-surface elevation at points: (a)  $y=2.05$  (corresponding to  $1S$ ) and (b)  $y=5.88$  (corresponding to  $2S$ ) for the plane beach geometry (bold dashed line) and the conical island (bold line).

beach, obtained via the analytical model of Sammarco & Renzi (2008). Here the beach slope  $s=1/3$  is the same as that of the island flanks. The characteristic parameters of the slide,  $\sigma$  and  $\lambda$  do not vary too, as anticipated above. In the same figure 14(a,b) the time series at points  $1S$  and  $2S$  of the conical island, already depicted in figure 12(a,b), are reported again for easiness of comparison, in bold lines. Note that at both points  $1S$  and  $2S$  the maximum runup (and minimum drawdown) of the first incoming waves is larger in the plane beach than in the conical island, even if the characteristic parameters of the slide are the same in both the geometries. This feature is again consequence of the fact that perfect wave trapping is possible only in a straight geometry. While on the plane beach energy is all trapped along the coast, due to the propagation of edge waves along the shoreline, in the circular geometry of the conical island perfect trapping is not possible. All frequencies, even the smallest ones, leak some amount of energy to infinity, resulting in attenuation of the maximum wave height around the coast. This crucial result has been also shown to occur in the experiments of Di Risio *et al.* (2009b).

## 5. Conclusion

An analytical forced two-horizontal-dimension model has been developed to analyse the distinguishing features of landslide tsunamis propagating around a conical island–continental shelf system. Two fields of wave motion are defined, the near field, i.e.

the inner zone with variable depth, and the far field, i.e. the outer zone with constant depth. The long wave equation is solved in each of the two fields separately. The free-surface elevation in the whole domain is then found by matching at the common boundary the solutions for the two fields. As many other linear-system responses to transient excitations, the free-surface elevation in each field is given by integrating the solution of the homogeneous wave equation multiplied by the forcing factor proper to the field and dependent on the characteristics of the slide. The resulting perturbation of the free surface is made by transient waves propagating radially and transient local waves almost trapped. The occurrence of a leading elevation wave travelling offshore at large times is shown, its amplitude decaying as  $O(t^{-1/2})$ , i.e. faster than the leading Airy wave generated by a transient disturbance in a two-dimensional ocean of constant depth.

Experimental comparison shows the validity of the model in reproducing the overall fluid behaviour. The tsunami generation mechanism is analysed for a subaerial slide. Just after the landslide has entered the water, the first perturbation leaves the origin as a positive N-wave. The wave profile near the generation zone resembles that of tsunamis along a plane beach. The free-surface runup at the shoreline induced by a half-submerged slide has been also investigated. Near the landslide the maximum runup is reached by the first crest of the incoming wavetrain, while far from the generation zone the highest wave is always shifted towards the middle of the incoming group. This is due to the excitation of edge-wave-like components of small frequency, for which the energy is almost trapped along the shore. However, unlike tsunamis propagating along an indefinite plane beach, where edge-wave energy is all trapped along the shoreline, tsunamis around a conical island propagate energy also in the offshore direction. As a consequence, the waves travelling along the shoreline of a conical island are characterized by smaller runup than those generated by a similar landslide along a plane beach with the same slope.

This work was funded by the Italian Ministry of Research (MIUR) under the research project ‘Development and validation of hydraulic and geologic tools for supporting a Tsunami Early Warning System. Implementation to the Stromboli (Eolie) landslide case’ (PRIN-2007). Experimental data provided by Dr M. Di Risio have been very useful for experimental comparison. Fruitful discussions with Dott. G. Bellotti are also kindly acknowledged.

## Appendix A. The confluent Heun equation

The CHE in its natural general form is (see Slavyanov 1995)

$$R_{rr}(r) + \left( \sum_{i=1}^2 \frac{A_i}{r - r_i} + E_0 \right) R_r(r) + \left( \sum_{i=1}^2 \frac{C_i}{r - r_i} + \sum_{i=1}^2 \frac{B_i}{(r - r_i)^2} + D_0 \right) R(r) = 0. \quad (\text{A } 1)$$

In the latter equation,  $R(r) : \mathbb{R} \rightarrow \mathbb{C}$  is the dependent function,  $A_i, B_i, C_i$  ( $i = 1, 2$ ),  $D_0$  and  $E_0$  are given coefficients. The CHE has two regular singular points at  $r = r_1$  and  $r = r_2$ , while  $r = \infty$  is an irregular singular point.

Let the coefficients in (A 1) be as follows:

$$A_1 = A_2 = 1; \quad B_1 = D_0 = 0; \quad C_1 = \lambda^2, C_2 = 0; \quad B_2 = -n^2; \quad E_0 = 0,$$

with  $n \in \mathbb{N}$  and  $\lambda \in \mathbb{C}$ . Also, set the two regular singular points respectively at  $r_1 = r_0 > 0$  and  $r_2 = 0$ , while leaving the remaining irregular singularity at infinity. Finally, restrict the domain of interest to  $r > r_0$ . With these positions, (A 1) becomes

$$R_{n,rr} + \left(\frac{1}{r} + \frac{1}{r - r_0}\right) R_{n,r} + \left[\frac{\lambda^2}{r - r_0} - \frac{n^2}{r^2}\right] R_n = 0. \tag{A 2}$$

As seen in §2, this equation describes the behaviour of the radial part  $R(r)$  of the free-surface elevation  $\zeta(r, \theta, t)$  around a conical island of radius  $r_0$ ,  $\lambda$  representing the complex wave frequency and  $n$  the order of the angular modes.

A.1. *Solution*

To find the two independent solutions of the CHE (A 2), we shall use the following change of variables

$$\xi = 1 - \frac{r_0}{r}, \quad Z_n(\xi; \lambda) = R_n(r; \lambda) \tag{A 3}$$

first suggested by Zhang & Zhu (1994), who already solved (A 2), but only finding one of the two independent solutions. Note that Zhang & Zhu (1994) called their result ‘new’, without explicitly referring to the theory of confluent Heun functions originally developed by Heun (1899) and then tuned by Slavyanov (1995). Here we pursue a slightly different deduction of the solution, which eventually will enable us to investigate the asymptotic behaviour of the confluent Heun functions for large parameter  $\lambda$ . By using (A 3) the regular singular point at  $r = r_0$  is mapped to  $\xi = 0$ , while the irregular singularity at infinity is mapped to  $\xi = 1$  and (A 2) becomes

$$Z_{n,\xi\xi} + \frac{p(\xi)}{\xi} Z_{n,\xi} + \frac{q(\xi)}{\xi^2} Z_n = 0, \tag{A 4}$$

where

$$p(\xi) = 1, \quad q(\xi) = \frac{\lambda^2 r_0 \xi - n^2 \xi^2 (1 - \xi)}{(1 - \xi)^3}. \tag{A 5}$$

We shall now employ the Frobenius’ method of power series to find the two independent solutions of (A 4) about the regular singular point  $\xi = 0$ . Let us assume

$$Z(\xi; \lambda) = \xi^\rho \sum_{m=0}^{\infty} a_{nm}(\rho; \lambda) \xi^m, \tag{A 6}$$

with  $\rho$  and  $a_{nm}$  being respectively the index and the coefficients of the Frobenius expansion (A 6), still unknown. Also, since both the polynomials  $p(\xi)$  and  $q(\xi)$  are analytic at  $\xi = 0$ , they can be expanded in Taylor series about the origin:

$$\left\{ \begin{matrix} p(\xi) \\ q(\xi) \end{matrix} \right\} = \sum_{k=0}^{\infty} \left\{ \begin{matrix} p_k \\ q_k \end{matrix} \right\} \xi^k, \quad \left\{ \begin{matrix} p_k \\ q_k \end{matrix} \right\} = \left\{ \begin{matrix} 0 \\ -n^2(k - 1) + \frac{\lambda^2 r_0}{2} (k + k^2) \end{matrix} \right\}, \tag{A 7}$$

$k \geq 1$ , with  $p_0 = 1$  and  $q_0 = 0$ . Substitution of both the series expansions (A 6) and (A 7) into (A 4) gives

$$\sum_{m=0}^{\infty} (m + \rho)(m + \rho - 1) a_{nm} \xi^{(m+\rho-2)} + \sum_{m,k=0}^{\infty} p_k \xi^k (m + \rho) a_{nm} \xi^{(m+\rho-2)} + \sum_{m,k=0}^{\infty} q_k \xi^k a_{nm} \xi^{(k+\rho-2)} = 0, \tag{A 8}$$



where  $\rho$  and the  $a_{nm}$  are unknown. Equation (A 8) is a polynomial expression which involves powers of  $\xi$ . For (A 8) to be satisfied  $\forall \xi \in (0, 1)$ , we must require that the coefficients of each power of  $\xi$  are zero. Starting from the lowest power  $\xi^{\rho-2}$  (obtained with  $m = k = 0$ ) we have

$$a_{n0} [\rho^2 + (p_0 - 1)\rho + q_0] = 0, \tag{A 9}$$

which is the indicial equation. Setting the arbitrary parameter  $a_{n0} = 1$ , the roots  $\rho_1, \rho_2$  of the indicial equation (A 9) give the two indexes of the series expansion (A 6). With  $p_0 = 1$  and  $q_0 = 0$ , (A 9) simply becomes  $\rho^2 = 0$ . Hence  $\rho_1 = \rho_2 = 0$  are two coinciding indexes. According to Frobenius' theory, in this case only one independent solution of (A 4) has the sought form (A 6). The other solution has instead logarithmic terms and can be obtained only via further investigation (see Bender & Orszag 1978). Back to the first independent solution (A 6), the unknown terms  $a_{nm}(\rho; \lambda)$  are to be found by setting to zero the remaining coefficients of the polynomial expression (A 8). Hence we get

$$a_{nm}(\rho; \lambda) = \frac{1}{(m + \rho)^2} \sum_{k=1}^m a_{n,m-k}(\rho) \left[ n^2(k - 1) - \frac{\lambda^2 r_0}{2} (k + k^2) \right], \quad m = 1, 2, \dots \tag{A 10}$$

Then by substituting  $\rho = 0$  in the latter relations we get the sought expression for the coefficients  $a_{nm}(\lambda) = a_{nm}(\rho = 0; \lambda)$  of the series expansion (A 6):

$$a_{nm}(\lambda) = \frac{1}{m^2} \sum_{k=1}^m a_{n,m-k} \left[ n^2(k - 1) - \frac{\lambda^2 r_0}{2} (k + k^2) \right], \quad m = 1, 2, \dots \tag{A 11}$$

so that the first independent solution of the transformed equation (A 4) is

$$Z_n(\xi; \lambda) = \sum_{m=0}^{\infty} a_{nm}(\lambda) \xi^m, \tag{A 12}$$

with the  $a_{nm}$  given by (A 11). The Confluent Heun function of first kind and order  $n$  in terms of  $r$  (recall A 3) is

$$Hc_n^{(1)}(r/r_0; \lambda) \equiv Z_n(\xi; \lambda) = \sum_{m=0}^{\infty} a_{nm}(\lambda) \left( 1 - \frac{r_0}{r} \right)^m, \tag{A 13}$$

and it represents the first independent solution of the governing equation (A 2). As done in §1, the parametric dependence on the radius  $r_0$  is further omitted for the sake of brevity. The series solution (A 13) has been checked numerically against the result of Zhang & Zhu (1994) showing perfect agreement. The second independent solution can now be found by differentiating the Frobenius series (A 6) with respect to the index  $\rho$ . In so doing, define the shorthand notation

$$L \cdot = (\cdot)_{\xi\xi} + \frac{p(\xi)}{\xi} (\cdot)_{\xi} + \frac{q(\xi)}{\xi^2} (\cdot),$$

such that (A 4) can be rewritten as  $LZ(\xi; \lambda) = 0$ . The general Frobenius expansion (A 6) satisfies

$$LZ(\xi; \lambda) = a_{n0} \xi^{\rho-2} \rho^2. \tag{A 14}$$

Indeed, by setting  $\rho = 0$ , the right hand of the latter expression vanishes and the polynomial expression (A 8) is obtained again, leading back to the first independent

solution. However, differentiating (A 14) with respect to the index  $\rho$  and then substituting  $\rho = 0$  yield

$$L \left[ \frac{\partial Z}{\partial \rho} \Big|_{\rho=0} \right] = 0, \tag{A 15}$$

where  $Z$  is given by (A 6). Therefore

$$\frac{\partial Z}{\partial \rho} \Big|_{\rho=0} = \ln(\xi) \sum_{m=0}^{\infty} a_{nm}(\lambda) \xi^m + \sum_{m=0}^{\infty} b_{nm}(\lambda) \xi^m$$

is also an independent solution of (A 4). The series coefficients

$$b_{nm}(\lambda) = \frac{\partial a_{nm}(\rho; \lambda)}{\partial \rho} \Big|_{\rho=0}$$

must satisfy the following relationship in order to be a solution of (A 15):

$$b_{nm}(\lambda) = \frac{1}{m^2} \sum_{k=1}^m b_{m-k} \left[ n^2(k-1) - \frac{\lambda^2 r_0}{2} (k+k^2) \right] - \frac{2}{m} a_{nm}(\lambda), \quad m = 1, 2, \dots \tag{A 16}$$

with  $b_{n0} = 0$  and the  $a_{nm}$  given by (A 11). Back to the original variable  $r$  via the transforms (A 3), the second independent solution to (A 2) is then the Confluent Heun function of second kind and order  $n$

$$Hc_n^{(2)}(r; \lambda) = \ln \left( 1 - \frac{r_0}{r} \right) \sum_{m=0}^{\infty} a_{nm}(\lambda) \left( 1 - \frac{r_0}{r} \right)^m + \sum_{m=0}^{\infty} b_{nm}(\lambda) \left( 1 - \frac{r_0}{r} \right)^m. \tag{A 17}$$

Finally, the general solution of (A 2) is the linear combination of the two independent ones, respectively (A 13) and (A 17):

$$R_n(r; \lambda) = \alpha_n Hc_n^{(1)}(r; \lambda) + \beta_n Hc_n^{(2)}(r; \lambda).$$

### A.2. Wronskian

Let us rewrite the CHE (A 2) in the Sturm–Liouville form

$$\frac{d}{dr} (hr R_{n,r}) + \left[ (i\omega)^2 r - \frac{n^2 h}{r} \right] R_n = 0, \tag{A 18}$$

where  $h = r - r_0$ ,  $\omega = i\lambda$ . The two linearly independent solutions of (A 18),  $R_n^{(1)} = Hc_n^{(1)}(r; i\omega)$  and  $R_n^{(2)} = Hc_n^{(2)}(r; i\omega)$  satisfy then

$$\frac{d}{dr} (hr R_{n,r}^{(1)}) + \left[ (i\omega)^2 r - \frac{n^2 h}{r} \right] R_n^{(1)} = 0$$

and

$$\frac{d}{dr} (hr R_{n,r}^{(2)}) + \left[ (i\omega)^2 r - \frac{n^2 h}{r} \right] R_n^{(2)} = 0$$

respectively. Now multiplying the first of the latter equations by  $R_n^{(2)}$ , the second one by  $R_n^{(1)}$  and then subtracting the two results, we get

$$\frac{d}{dr} (hr R_{n,r}^{(1)} R_n^{(2)} - hr R_{n,r}^{(2)} R_n^{(1)}) = 0.$$

Integration of this differential equation with respect to  $r$  provides

$$R_n^{(1)} R_{n,r}^{(2)} - R_{n,r}^{(1)} R_n^{(2)} = -\frac{A}{r(r-r_0)}, \tag{A 19}$$

where the left-side term is indeed the Wronskian  $W[R_n^{(1)}, R_n^{(2)}]$  of the two independent solutions. The integration constant  $A$  can be found by directly evaluating the Wronskian  $W$  as  $r$  tends to  $r_0$ . For  $r \rightarrow r_0$  the behaviour of the two functions  $R_n^{(1)} = Hc_n^{(1)}(r; i\omega)$  and  $R_n^{(2)} = Hc_n^{(2)}(r; i\omega)$  is defined by truncating the series solutions (A 13) and (A 17) respectively to terms of order  $O(1 - r_0/r)$ . This yields

$$R_n^{(1)} = Hc_n^{(1)}(r; i\omega) \simeq 1 + \omega^2 r_0 \left(1 - \frac{r_0}{r}\right)$$

for the first solution and

$$R_n^{(2)} = Hc_n^{(2)}(r; i\omega) \simeq \ln\left(1 - \frac{r_0}{r}\right) \left[1 + \omega^2 r_0 \left(1 - \frac{r_0}{r}\right)\right] - 2\omega^2 r_0 \left(1 - \frac{r_0}{r}\right)$$

for the second solution. Derivatives  $R_{n,r}^{(1)}$  and  $R_{n,r}^{(2)}$  for  $r \rightarrow r_0$  can be evaluated by differentiating the above expressions with respect to  $r$ . Then (A 19) becomes

$$W = \frac{r_0}{r(r - r_0)} + \omega^4 \frac{r_0^3}{r^3} (r - r_0) = -\frac{A}{r_0(r - r_0)},$$

which in the limit for  $r \rightarrow r_0$  yields  $A = -r_0$ , i.e.

$$W [Hc_n^{(1)}(r; i\omega), Hc_n^{(2)}(r; i\omega)] = W(r) = \frac{r_0}{r(r - r_0)}. \tag{A 20}$$

A.3. Asymptotic behaviour for large parameter  $\lambda = i\omega$

Consider the CHE (A 2), whose independent solutions are the two confluent Heun functions  $Hc_n^{(1)}(r; \lambda)$  and  $Hc_n^{(2)}(r; \lambda)$  of first and second kind respectively. Now let the parameter  $\lambda = i\omega$ , with  $\omega \in \mathbb{C}$ . Then, the  $a_{nm}(\lambda = i\omega)$  are

$$a_{n,0} = 1, \quad a_{n,1} = \omega^2 r_0, \quad a_{n,2} = \frac{1}{4} \omega^4 r_0^2 + \frac{3}{4} \omega^2 r_0 + \frac{1}{4} n^2$$

$$a_{n,3} = \frac{1}{36} \omega^6 r_0^3 + \frac{5}{12} \omega^4 r_0^2 + \left(\frac{5}{36} n^2 + \frac{2}{3}\right) \omega^2 r_0 + \frac{2}{9} n^2.$$

For very large  $\omega$  we retain only the higher order terms in the preceding expansions, thus getting the following approximated behaviour for the  $a_{nm}$ :

$$a_{nm} \simeq \frac{(\omega \sqrt{r_0})^{2m}}{(m!)^2}, \quad m = 1, 2, \dots \tag{A 21}$$

Therefore, to the crudest approximation,

$$Hc_n^{(1)}(r; i\omega) \simeq \sum_{m=0}^{\infty} \frac{(x/2)^{2m}}{(m!)^2} = I_0(x)$$

where  $x = 2\omega \sqrt{r_0(1 - r_0/r)}$  and  $I_0(x)$  is the modified Bessel function of first kind and order zero. Hence, for large  $\omega$

$$Hc_n^{(1)}(r; i\omega) \simeq I_0 \left[ 2\omega \sqrt{r_0 \left(1 - \frac{r_0}{r}\right)} \right]. \tag{A 22}$$

The second independent solution of the CHE  $Hc_n^{(2)}$  has coefficients  $b_{nm}$  given by (A 16), which letting  $\lambda = i\omega$  and  $\omega \rightarrow \infty$  can be approximated by

$$b_{n,0} = 0, \quad b_{n,m} \simeq -2 \left(1 + \frac{1}{2} + \frac{1}{3} + \dots + \frac{1}{m}\right) \frac{1}{(m!)^2} (\omega \sqrt{r_0})^{2m}, \quad m = 1, 2, \dots \tag{A 23}$$

Therefore to the crudest approximation for  $\omega \rightarrow \infty$ , recalling (A 17) and (A 22), we obtain

$$Hc_n^{(2)}(r; i\omega) \simeq 2 \left\{ \ln \left( \frac{x}{2\omega\sqrt{r_0}} \right) I_0(x) - \left[ \frac{x^2}{4} + \left( 1 + \frac{1}{2} \right) \frac{1}{(2!)^2} \left( \frac{x^2}{4} \right)^2 + \left( 1 + \frac{1}{2} + \frac{1}{3} \right) \frac{(x^2/4)^3}{(3!)^2} + \dots \right] \right\}, \quad (\text{A } 24)$$

with  $x = 2\omega\sqrt{r_0(1 - r_0/r)}$ . Now, the terms inside the square brackets of the latter equation can be further expressed as

$$\frac{x^2}{4} + \left( 1 + \frac{1}{2} \right) \frac{1}{(2!)^2} \left( \frac{x^2}{4} \right)^2 + \dots = K_0(x) + \left[ \ln \left( \frac{x}{2} \right) + \gamma \right] I_0(x),$$

with  $\gamma = 0.577 \dots$  and  $K_0$  the modified Bessel function of second kind and order zero (see Abramowitz & Stegun 1972). Hence expression (A 24) can be simplified as

$$Hc_n^{(2)}(r; i\omega) \simeq 2 \left\{ I_0 \left[ 2\omega\sqrt{r_0 \left( 1 - \frac{r_0}{r} \right)} \right] \left[ \ln \left( \frac{1}{\omega\sqrt{r_0}} \right) - \gamma \right] - K_0 \left[ 2\omega\sqrt{r_0 \left( 1 - \frac{r_0}{r} \right)} \right] \right\}, \quad (\text{A } 25)$$

for large  $\omega \in \mathbb{C}$ . Moreover, in the complex half-plane  $|\arg(\omega)| < \pi/2$ ,  $K_0 \rightarrow 0$  for large  $\omega$ . The asymptotic expansion (A 25) can be further approximated to the leading behaviour

$$Hc_n^{(2)}(r; i\omega) \simeq -2I_0 \left[ 2\omega\sqrt{r_0 \left( 1 - \frac{r_0}{r} \right)} \right] \ln(\omega\sqrt{r_0}), \quad (\text{A } 26)$$

for large  $\omega$ , with  $|\arg(\omega)| < \pi/2$ .

#### A.4. Behaviour for small parameter $\lambda$

The behaviour of the confluent Heun functions for small  $\lambda$  can be obtained by keeping only the first term in the relevant series expansions, with the argument  $r/r_0$  regarded as a parameter. Hence the confluent Heun function of the first kind (A 13) becomes

$$Hc_n^{(1)}(r; \lambda) \simeq Hc_n^{(1)}(r; 0) + O(\lambda^2), \quad (\text{A } 27)$$

while

$$Hc_n^{(2)}(r; \lambda) \simeq Hc_n^{(2)}(r; 0) + O(\lambda^2), \quad (\text{A } 28)$$

is the approximation of the confluent Heun function of second kind (A 17). Asymptotic expansions of derivatives for small  $\lambda$  are defined accordingly, giving respectively

$$Hc_{n,r}^{(1)}(r; \lambda) \simeq Hc_{n,r}^{(1)}(r; 0) + O(\lambda^2)$$

and

$$Hc_{n,r}^{(2)}(r; \lambda) \simeq Hc_{n,r}^{(2)}(r; 0) + O(\lambda^2).$$

## Appendix B. Complex integrals evaluation

### B.1. Evaluation of the inner integral of (3.1)

Consider the integral in the far field

$$\int_{c-i\infty}^{c+i\infty} f_n(\omega) e^{\omega t} d\omega, \quad (\text{B } 1)$$

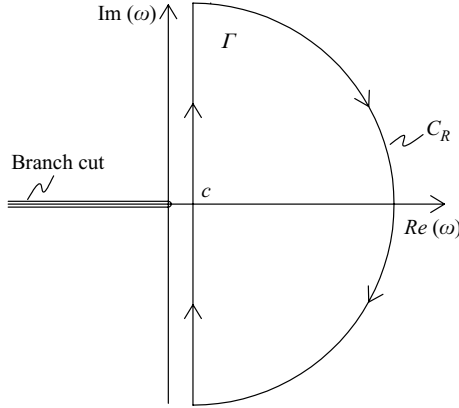


FIGURE 15. Integration contour  $\Gamma$  for  $t < 0$  and the semicircular contour  $C_R$ .

where

$$f_n(\omega) = \frac{F_n(\rho; \omega) Hc_n^{(1)}(\rho; i\omega) K_n(\omega r / \sqrt{h_b})}{\Delta_n^{(1)}(\omega)}. \tag{B 2}$$

Here  $\rho \in (r_0, b)$  and  $r \in (b, \infty)$  are regarded as parameters, the forcing function  $F_n$  is given by (2.17) and the denominator  $\Delta_n^{(1)}$  by (2.27).  $c$  is a positive real constant. A branch cut on the negative real axis is introduced to avoid multi-valuedness of  $K_n$  (see Abramowitz & Stegun 1972).

For  $t < 0$ , take a large semicircular contour  $C_R$  on the half-plane

$$\Omega = \{\omega \in \mathbb{C} : |\arg(\omega)| < \pi/2, \omega \neq 0\},$$

to form the closed circuit  $\Gamma$ , as depicted in figure 15. Hence

$$\int_{c-i\infty}^{c+i\infty} f_n(\omega) e^{\omega t} d\omega = \oint_{\Gamma} f_n e^{\omega t} d\omega - \int_{C_R} f_n e^{\omega t} d\omega. \tag{B 3}$$

Note that in the complex domain  $\Omega$  each of the functions at the numerator of  $f_n$ , expression (B 2), are entire functions of  $\omega$  ( $K_n$  has a pole at  $\omega = 0 \notin \Omega$ ). The denominator  $\Delta_n^{(1)}$  (2.27) of the integrand  $f_n$  has no zeros in the same complex domain, as shown in figure 16(a,b). Since no poles are found for  $f_n$ ,  $\oint_{\Gamma} f_n e^{\omega t} = 0$ , as a result of Cauchy's theorem. On the large semicircular contour  $C_R$  the function  $F_n$  (2.17) at the numerator of the integrand  $f_n$  (3.2) can be expanded for large  $\omega$  as

$$F_n(\rho; \omega) \simeq -2\Pi_n(r - r_s),$$

i.e. a constant, having used the approximation  $\text{erf}(-x) \simeq -1 + e^{-x^2} / \sqrt{\pi} x$  for large  $x$ . Also, recall the asymptotic expression (A 22),

$$Hc_n^{(1)}(r; i\omega) \simeq I_0\left(2\omega\sqrt{r_0(1 - r_0/r)}\right),$$

as shown in Appendix A.3. Finally, the modified Bessel functions of first and second kind can be approximated to the leading order by

$$I_n(x) \simeq \frac{e^x}{\sqrt{2\pi x}}, \quad \text{if } |\arg(x)| < \frac{\pi}{2}$$

and

$$K_n(x) \simeq \frac{e^{-x}}{\sqrt{\frac{2}{\pi} x}}, \quad \text{if } |\arg(x)| < \frac{3}{2}\pi$$

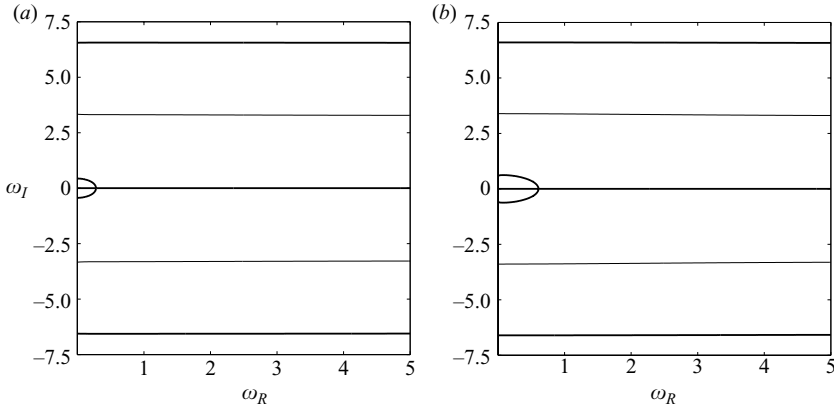


FIGURE 16. Contour plots of the curves  $\text{Re}\{\Delta_n^{(1)}(\omega)\} = 0$  (solid line) and  $\text{Im}\{\Delta_n^{(1)}(\omega)\} = 0$  (bold line) in the complex  $\omega = \omega_R + i\omega_I$  plane, for modal order  $n = 0$  (a) and  $n = 1$  (b). Parameters are  $r_0 = 11.82$ ,  $b = 25.43$ . Complex zeros of  $\Delta_n^{(1)}$ , expression (2.27), occur at the points of intersection of the two curves  $\text{Re}\{\Delta_n^{(1)}\} = 0$  and  $\text{Im}\{\Delta_n^{(1)}\} = 0$ . Note that no point of intersection is found in the domain considered.

respectively (see Abramowitz & Stegun 1972). By substituting the asymptotic expansions of  $F_n$ ,  $Hc_n^{(1)}$ ,  $I_n$  and  $K_n$  for large  $\omega$  into the integrand function  $f_n(\omega)$  (B 2), we get the leading behaviour of  $f_n$  for large  $\omega$ :

$$f_n(\omega) \simeq \frac{e^{-(\alpha\omega+\beta)}}{\omega}, \tag{B 4}$$

where

$$\alpha = 2\sqrt{r_0} \left( \sqrt{1 - \frac{r_0}{b}} - \sqrt{1 - \frac{r_0}{\rho}} \right) \tag{B 5}$$

and

$$\beta = h_b^{-1/2}(r - b) \tag{B 6}$$

are constant for fixed  $\rho$  and  $r$ . Since  $\rho \in (r_0, b)$  and  $r \in (b, \infty)$ , both the terms  $\alpha$  (B 5) and  $\beta$  (B 6) are positive. Now let us substitute  $\omega = Re^{i\vartheta}$ ,  $|\vartheta| < \pi/2$  inside (B 4); since  $\text{Re}\{\omega\} = R \cos \vartheta > 0$ , the asymptotic expansion (B 4) on the large semicircular contour  $C_R$  is a negative exponential of  $R$ . As a result  $|f_n| \rightarrow 0$  in the limit  $R \rightarrow \infty$ . The application of the Jordan's lemma gives then  $\int_{C_R} f_n e^{\omega t} d\omega = 0$ , so that

$$\int_{c-i\infty}^{c+i\infty} f_n(\omega) e^{\omega t} d\omega = 0,$$

for  $t < 0$ .

For  $t > 0$ , consider the new integration path  $\Gamma \subseteq \Omega$  shown in figure 17. As above, we may write

$$\int_{c-i\infty}^{c+i\infty} f_n(\omega) e^{\omega t} d\omega = \left( \oint_{\Gamma} - \int_{\Gamma^+} - \int_{\Gamma^-} - \int_{\Gamma_\epsilon} \right) f_n(\omega) e^{\omega t} d\omega, \tag{B 7}$$

where the straight lines  $\Gamma^+$  and  $\Gamma^-$  are parallel to the real axis at  $\text{Im}\{\omega\} = \pm \infty$  respectively, and the line  $\Gamma_\epsilon$  lies just on the right of the imaginary axis, with  $\epsilon \ll 1$  (see figure 17);  $f_n(\omega)$  is still given by (B 2). As seen above, the integrand  $f_n$  has no poles for  $\omega \in \Omega$ . Hence application of the Cauchy theorem to the first integral gives

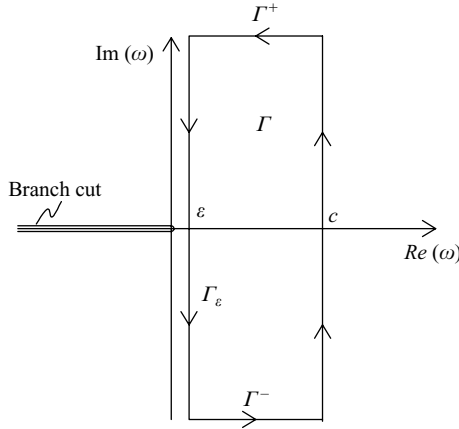


FIGURE 17. Integration contour  $\Gamma$  for  $t > 0$ .

$\oint_{\Gamma} f_n(\omega)e^{\omega t} d\omega = 0$ . Now, as  $\epsilon$  approaches zero, the second integral on the straight line  $\Gamma^+$  can be written as

$$\int_{\Gamma^+} f_n(\omega)e^{\omega t} d\omega = \lim_{\delta \rightarrow \infty} \int_c^{\epsilon} f_n(s + i\delta)e^{(s+i\delta)t} ds = \lim_{\delta \rightarrow \infty} e^{-\beta+i\delta(t-\alpha)} \int_c^{\epsilon} \frac{e^{s(t-\alpha)}}{s + i\delta} ds = 0, \quad (\text{B } 8)$$

having used the asymptotic formula (B 4) for  $f_n$ . Analogous considerations can be made on the third integral in (B 7), yielding  $\int_{\Gamma^-} f_n(\omega)e^{\omega t} d\omega = 0$ . Expression (B 7) becomes

$$\int_{c-i\infty}^{c+i\infty} f_n(\omega)e^{\omega t} d\omega = \int_{\epsilon-i\infty}^{\epsilon+i\infty} f_n(\omega)e^{\omega t} d\omega.$$

Consider the transform

$$\omega = e^{i\pi/2} s, \quad (\text{B } 9)$$

which is a rotation of  $-90^\circ$  about the origin. The latter integral equation becomes then

$$\int_{c-i\infty}^{c+i\infty} f_n(\omega)e^{\omega t} d\omega = i \int_{-\infty-i\epsilon}^{+\infty-i\epsilon} f_n(is)e^{ist} ds \doteq i L_n(s). \quad (\text{B } 10)$$

In the limit  $\epsilon \rightarrow 0$ , the new integration path becomes slightly deformed due to the presence of the pole for  $K_n$  (see B 2) at  $\omega = 0$ . The branch cut is now placed on the positive imaginary axis after having applied the transform (B 9) (see figure 18). Hence we obtain

$$L_n(s) = \int_{-\infty-i\epsilon}^{+\infty-i\epsilon} f_n(is)e^{ist} ds = \left( \int_{-\infty}^0 + \int_0^\infty + \int_{C_\delta} \right) f_n(is)e^{ist} ds, \quad (\text{B } 11)$$

$C_\delta$  being a small semicircle of radius  $\delta \ll 1$  surrounding the origin of the complex plane, as depicted in figure 18. To evaluate the integral on the semicircle  $C_\delta$ , consider

$$f_n(is) = \frac{F_n(\rho; is)Hc_n^{(1)}(\rho; s)K_n(isr/\sqrt{h_b})}{\Delta_n^{(1)}(is)}, \quad (\text{B } 12)$$

as  $s \rightarrow 0$ . The forcing term  $F_n$  (2.17) at the numerator of (B 12) can be approximated as  $F_n(\rho; is) \simeq -2(\rho - r_s)e^{-(\rho - r_s)^2}$  for small  $s$ ,  $\rho$  being still regarded as a parameter; the

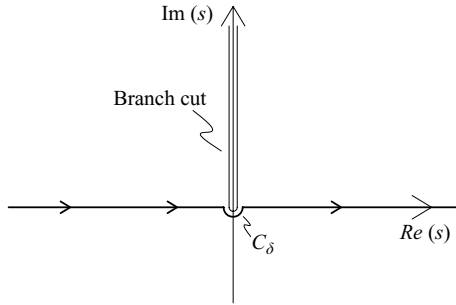


FIGURE 18. Integration path (bold line) for (B 10). Note that the presence of the pole for  $K_n$  at  $\omega = 0$  induces a deformation of the path, generating the small semicircle  $C_\delta$ .

asymptotic expansion of the modified Bessel functions of second kind is instead

$$\left\{ \begin{matrix} K_0(x) \\ K_n(x) \end{matrix} \right\} \simeq \left\{ \begin{matrix} -\ln(x) \\ \frac{1}{2}(n-1)! \left(\frac{x}{2}\right)^{-n} \end{matrix} \right\}$$

for small argument  $x \in \mathbb{C}$  and  $n = 1, 2, \dots$  (see Abramowitz & Stegun 1972). Finally, the confluent Heun function of first kind can be expanded for small parameter  $s$  as shown in Appendix A.4, yielding  $Hc_n^{(1)}(r; s) \simeq Hc_n^{(1)}(r; 0) + O(s^2)$ , where the first expansion term is a finite value depending on the parameter  $r/r_0 \in (1, \infty)$ . The derivative of the confluent Heun function of the first kind  $Hc_{n,r}^{(1)}$  is defined accordingly  $Hc_{n,r}^{(1)}(r; s) \simeq Hc_{n,r}^{(1)}(r; 0) + O(s^2)$ . Substituting the approximated forms for the forcing function  $F_n$ , the modified Bessel function  $K_n$  and the confluent Heun function  $Hc_n^{(1)}$  into both the numerator and the denominator  $\Delta_n^{(1)}(is)$  of (B 12) yields

$$f_0(is) \simeq 2b(\rho - r_s) e^{-(\rho - r_s)^2} \ln\left(\frac{isr}{\sqrt{h_b}}\right) \tag{B 13}$$

for  $n = 0$  and

$$f_n(is) \simeq \frac{Hc_n^{(1)}(\rho; 0) \left(\frac{b}{r}\right)^n \left[-2(\rho - r_s) e^{-(\rho - r_s)^2}\right]}{\frac{n}{b} Hc_n^{(1)}(b; 0) + Hc_{n,r}^{(1)}(b; 0)} = O(1) \tag{B 14}$$

for  $n = 1, 2, \dots, s \ll 1$ . Note that in (B 13) and (B 14)  $r$  and  $\rho$  are to be regarded as parameters. With the approximated forms (B 13) and (B 14) the integral on the semicircle  $C_\delta$  (third of B 11) becomes

$$\int_{C_\delta} f_0(is) e^{ist} ds \simeq 2b(\rho - r_s) e^{-(\rho - r_s)^2} \int_{C_\delta} \ln\left(\frac{isr}{\sqrt{h_b}}\right) ds \tag{B 15}$$

for  $n = 0$  and

$$\int_{C_\delta} f_n(is) e^{ist} ds \simeq \int_{C_\delta} O(1) ds \tag{B 16}$$

for  $n = 1, 2, \dots$  respectively. Making use of the parametric transform  $s = \delta e^{i\phi}$ ,  $\phi \in (-\pi, 0)$ , and letting  $\delta \rightarrow 0$  yield

$$\int_{C_\delta} f_0(is) e^{ist} ds \propto \delta \int_{-\pi}^0 \ln(i\delta e^{i\phi}) e^{i\phi} d\phi \rightarrow 0$$



for (B 15) and

$$\int_{C_\delta} f_n(is) e^{ist} ds \propto \delta \int_{-\pi}^0 O(1) e^{i\phi} d\phi \rightarrow 0$$

for (B 16). Hence the integral form (B 11) simplifies into

$$L_n(s) = \int_{-\infty}^{\infty} f_n(is) e^{ist} ds,$$

and the Laplace integral (B 10) becomes

$$\int_{c-i\infty}^{c+i\infty} f_n(\omega) e^{\omega t} d\omega = i L_n(s) = i \int_{-\infty}^{\infty} f_n(is) e^{ist} ds.$$

B.2. Evaluation of the integral (3.14)

Consider the complex integral

$$\int_{c-i\infty}^{c+i\infty} f_{jn}(\rho, \omega) d\omega, \quad j = 1, 2,$$

where

$$f_{1n}(\rho, \omega) = F_n(\rho; \omega) \left[ Hc_n^{(1)}(\rho; i\omega) \frac{\Delta_n^{(2)}(\omega)}{\Delta_n^{(1)}(\omega)} - Hc_n^{(2)}(\rho; i\omega) \right] Hc_n^{(1)}(r; i\omega)$$

and

$$f_{2n}(\rho, \omega) = F_n(\rho; \omega) \left[ Hc_n^{(1)}(\rho; i\omega) Hc_n^{(2)}(r; i\omega) - Hc_n^{(2)}(\rho; i\omega) Hc_n^{(1)}(r; i\omega) \right].$$

In the latter expressions,  $F_n$  is the forcing function (2.17), while  $\Delta_n^{(1,2)}$  are given by (2.27);  $\rho$  and  $r$  are fixed parameters.

For  $t < 0$ , take the large semicircular contour  $C_R$  depicted in figure 15. Hence

$$\int_{c-i\infty}^{c+i\infty} f_{jn}(\rho, \omega) d\omega = \oint_{\Gamma} f_{jn} e^{\omega t} d\omega - \int_{C_R} f_{jn} e^{\omega t} d\omega,$$

where  $\Gamma$  is the closed circuit represented in figure 15. Since both  $f_{jn}$ ,  $j = 1, 2$  are entire functions of  $\omega \in \Omega$ , again  $\oint_{\Gamma} f_{jn} e^{\omega t} d\omega = 0$  by application of the Cauchy theorem. Furthermore, repeating the same algebra of the previous section, it is straightforward to show that  $|f_{jn}(\rho, \omega)| \rightarrow 0$  as  $|\omega| \rightarrow \infty$ . As a consequence of the Jordan lemma,  $\int_{C_R} f_{jn}(\rho, \omega) e^{\omega t} d\omega = 0$  and

$$\int_{c-i\infty}^{c+i\infty} f_{jn}(\omega) e^{\omega t} d\omega = 0, \quad j = 1, 2$$

for  $t < 0$ .

For  $t > 0$ , consider again the closed circuit shown in figure 17. As seen before

$$\int_{c-i\infty}^{c+i\infty} f_{jn} e^{\omega t} d\omega = \left( \oint_{\Gamma} - \int_{\Gamma^+} - \int_{\Gamma^-} - \int_{\Gamma_\epsilon} \right) f_{jn}(\omega) e^{\omega t} d\omega, \tag{B 17}$$

where  $\Gamma^+$  and  $\Gamma^-$  are two straight lines parallel to the real axis at  $\Im\{\omega\} = \pm \infty$  respectively, and the line  $\Gamma_\epsilon$  lies just on the right of the imaginary axis, with  $\epsilon \ll 1$  (see figure 17). Again, since the  $f_{jn}$  are entire functions of  $\omega \in \Omega$ , application of the Jordan lemma gives

$$\oint_{\Gamma} f_{jn} e^{\omega t} d\omega = 0.$$

Using the same argument of § 3.1, it is immediate to show that

$$\int_{\Gamma^{(+,-)}} f_{jn} e^{\omega t} d\omega = \lim_{\delta \rightarrow \infty} \int_{(c,\epsilon)}^{(\epsilon,c)} f_{jn}(s(+, -)i\delta) e^{(s(+,-)i\delta)t} ds = 0.$$

Therefore we are only left with

$$\int_{c-i\infty}^{c+i\infty} f_{jn} e^{\omega t} d\omega = \int_{\epsilon-i\infty}^{\epsilon+i\infty} f_{jn} e^{\omega t} d\omega,$$

$\epsilon \ll 1$ . With the change of variable  $s = e^{i\pi/2}\omega$ , the latter integral equation becomes

$$\int_{c-i\infty}^{c+i\infty} f_{jn} e^{\omega t} d\omega = i \int_{-\infty-i\epsilon}^{\infty-i\epsilon} f_{jn}(is) e^{ist} ds \doteq iL_{jn}(s), \tag{B 18}$$

where the new integration path is slightly below the real  $s$ -axis. Letting  $\epsilon \rightarrow 0$ , the integrals  $L_{jn}(s)$  are evaluated again on the deformed contour shown in figure 18, thus yielding

$$L_{jn}(s) = \left( \int_{-\infty}^{\infty} + \int_{C_\delta} \right) f_{jn} e^{st} ds,$$

where  $C_\delta$  is the semicircular path of radius  $\delta \ll 1$  (see again figure 18). Consider the two integrand functions

$$f_{1n}(\rho, is) = F_n(\rho; is) \left[ Hc_n^{(1)}(\rho; s) \frac{\Delta_n^{(2)}(is)}{\Delta_n^{(1)}(is)} - Hc_n^{(2)}(\rho; s) \right] Hc_n^{(1)}(r; s)$$

and

$$f_{2n}(\rho, is) = F_n(\rho, is) \left[ Hc_n^{(1)}(\rho; is) Hc_n^{(2)}(r; s) - Hc_n^{(2)}(\rho; s) Hc_n^{(1)}(r; s) \right].$$

With the limiting forms for  $F_n$ ,  $K_n$ ,  $Hc_n^{(1)}$  and  $Hc_n^{(2)}$  already used in the previous subsection, it is immediate to show that  $|f_{jn}(is)| = O(1)$ ,  $j = 1, 2, \dots$ , as  $s$  tends to zero. Once again  $\int_{C_\delta} f_{jn} e^{ist} ds = 0$  on the small semicircle  $C_\delta$ . Hence (B 18) can be rewritten as

$$\int_{c-i\infty}^{c+i\infty} f_{jn} e^{\omega t} d\omega = iL_{jn}(\rho) = i \int_{-\infty}^{\infty} f_{jn}(\rho, is) e^{ist} ds, \tag{B 19}$$

with  $f_{jn}, j = 1, 2$ , given by (3.12) and (3.13) respectively.

REFERENCES

ABRAMOWITZ, M. & STEGUN, I. A. 1972 *Handbook of Mathematical Functions*, Applied Mathematics Series, vol. 55. National Bureau of Standards.

BARDET, J.-P., SYNOLAKIS, C. E., DAVIES, H. L., IMAMURA, F. & OKAL, E. A. 2003 Landslide tsunamis: recent findings and research directions. *Pure Appl. Geophys.* **160**, 1793–1809.

BENDER, C. & ORSZAG, S. A. 1978 *Advanced Mathematical Methods for Scientist and Engineers*. McGraw-Hill.

BRUNS, H. J., MACGILLIVRAY, J. A., SYNOLAKIS, C. E., BENJAMINI, C., KELLER, J., KISCH, H. J., KLGEL, A. & VAN DER PLICHT, J. 2008 Geoarchaeological tsunami deposits at Palaikastro (Crete) and the Late Minoan IA eruption of Santorini. *J. Archeological Sci.* **35** (1), 191–212.

DI RISIO, M., BELLOTTI, G., PANIZZO, A. & DE GIROLAMO, P. 2009a Three-dimensional experiments on landslide generated waves at a sloping coast. *Coast. Engng* **56** (5–6), 659–671.

DI RISIO, M., DE GIROLAMO, P., BELLOTTI, G., PANIZZO, A., ARISTODEMO, F., MOLFETTA, M. & PETRILLO, A. F. 2009b Landslide-generated tsunamis runup at the coast of a conical island: new physical model experiments. *J. Geophys. Res.* **114** (C01009).

- FUJIMA, K., YULIADI, D., GOTO, C., HAYASHI, K. & SHIGEMURA, T. 1995 Characteristics of long waves trapped by conical island. *Coast. Engng Japan* **38** (2), 111–132.
- GUZA, R. T. & DAVIS, R. E. 1974 Excitation of edge waves by waves incident on a beach. *J. Geophys. Res.* **79**, 1285–1291.
- HEUN, K. 1899 Zur Theorie der Riemann'schen Functionen zweiter Ordnung mit vier Verzweigungspunkten. *Mathematische Annalen* **33**, 161–179.
- KANOGLU, U. & SYNOLAKIS, C. E. 1998 Long wave runup on piecewise linear topographies. *J. Fluid Mech.* **374**, 1–28.
- LAUTENBACHER, C. C. 1970 Gravity wave refraction by islands. *J. Fluid Mech.* **41** (3), 655–672.
- LIU, P. L.-F., CHO, Y.-S., BRIGGS, M. J., KANOGLU, U. & SYNOLAKIS, C. E. 1995 Runup of solitary waves on a circular island. *J. Fluid Mech.* **302**, 259–285.
- LIU, P. L.-F., LYNETT, P. & SYNOLAKIS, C. E. 2003 Analytical solutions for forced long waves on a sloping beach. *J. Fluid Mech.* **478**, 101–109.
- LONGUET-HIGGINS, M. S. 1967 On the trapping of wave energy round islands. *J. Fluid Mech.* **29** (4), 781–821.
- LYNETT, P. & LIU, P. F. 2005 A numerical study of the runup generated by three-dimensional landslides. *J. Geophys. Res.* **110** (C003006).
- MEI, C. C., STIASSNIE, M. & YUE, D. K.-P. 2005 *Theory and Applications of Ocean Surface Waves*. World Scientific.
- MEYER, R. E. 1971 Resonance of unbounded water bodies. In *Mathematical Problems in the Geophysical Sciences* (ed. W. H. Reid), Lectures in Applied Mathematics, vol. 13. American Mathematical Society.
- PRESS, W. H., TEUKOLSKY, S. A., VETTERLING, W. T. & FLANNERY, B. P. 1986 *Numerical Recipes in Fortran 77*. Cambridge University Press.
- SAMMARCO, P. & RENZI, E. 2008 Landslide tsunamis propagating along a plane beach. *J. Fluid Mech.* **598**, 107–119.
- SLAVYANOV, S. Y. 1995 Confluent Heun equation. In *Heun's Differential Equation* (ed. A. Ronveaux), pp. 87–127. Oxford Science Publications.
- SMITH, R. & SPRINKS, T. 1975 Scattering of surface waves by a conical island. *J. Fluid Mech.* **72** (2), 373–384.
- SUMMERFIELD, W. 1971 Circular islands as resonators of long-wave energy. *Phil. Trans. R. Soc. Lond. Ser. A* **272**, 361–402.
- SYNOLAKIS, C. E., BERNARD, E. N., TITOV, V. V., KANOGLU, U. & GONZALEZ, F. I. 2008 Validation and verification of tsunami numerical models. *Pure Appl. Geophys.* **165** (11–12), 2197–2228.
- TINTI, S., MARAMAI, A., ARMIGLIATO, A., GRAZIANI, L., MANNUCCI, A., PAGNONI, G. & ZANIBONI, F. 2005 Observations of physical effects from tsunamis of December 30, 2002 at Stromboli volcano, southern Italy. *Bull. Volcanol.* **68** (5), 450–461.
- TINTI, S. & VANNINI, C. 1995 Tsunami trapping near circular islands. *Pure Appl. Geophys.* **144** (3/4), 595–619.
- TUCK, E. O. & HWANG, L. S. 1972 Long wave generation on a sloping beach. *J. Fluid Mech.* **51**, 449–461.
- YEH, H., LIU, P. L.-F., BRIGGS, M. & SYNOLAKIS, C. E. 1994 Tsunami catastrophe in Babi island. *Nature* **372**, 6503–6508.
- ZHANG, Y. & ZHU, S. 1994 New solutions for the propagation of long water waves over variable depth. *J. Fluid Mech.* **278**, 391–406.